Uncertainty Quantification Methodologies for Functional Data in Biomechanical Applications

by

Wenbo Sun

A dissertation submitted in partial fulfillment
of the requirements for the degree of
Doctor of Philosophy
(Industrial and Operations Engineering)
in The University of Michigan
2019

Doctoral Committee:

Professor Judy Jin, Co-Chair
Assistant Professor Matthew Plumlee, Co-Chair
Associate Professor Veronica Berrocal
Associate Professor Eunshin Byon

Wenbo Sun
sunwbgt@umich.edu
ORCID iD: 0000-0002-3811-5853

TABLE OF CONTENTS

LIST OF FIGURES

Figure

LIST OF TABLES

Table

ABSTRACT

Massive data are feasibly collected or generated with the rapid development of sensing, high computing and computer simulation technologies. Among various types of data, functional data plays an important role in tracking system behaviors in various applications. However, functional data often shows complex data uncertainty caused by multiple factors such as experimental conditions, subject characteristics or computer simulation settings. To better understand the system behaviors for decision-making, new methodologies are expected to systematically quantify the uncertainty of functional data. Specifically, three major research issues are studied in the dissertation. First, the problem of constructing confidence bands (also known as corridors in biomechanical applications) of univariate functional signals is discussed. An effective method is developed for confidence bands generation that applies principal component analysis (PCA). Rather than using existing empirical models to account for the effects of subject variables on functional responses, linear regression models are further built to model the relationship between extracted PC features and subject variables, which makes the effects of subject variables interpretable. The advantage of the resultant confidence bands is reflected by the narrower bands than those generated by existing techniques while keeping a high coverage rate of sampled experimental functional data. Second, a generic method is developed to construct confidence bands for bivariate functional data. The effect of subject variables is quantified by non-parametric B-spline fitting and a polynomial regression model, which is capable of capturing non-linear dependencies between the subject variables

and functional responses. Moreover, a Gaussian process model is developed to model the complicated covariance structure, which can fully consider between-subject and within-subject variability, auto-correlation between time points and cross-correlation between bivariate functional responses. Therefore, the constructed confidence bands can effectively capture the bivariate functional profile shape and functional variation patterns. As a byproduct, the developed model is effectively used for testing outliers of abnormal functional responses based on the property of the developed Gaussian process model. Third, a method to search for the optimal system design using an inexact computer simulation model with uncertainty quantification is developed. The uncertainty is quantified by specifying feasible regions instead of building a full probabilistic model, which makes the proposed method to be applicable when an emulator is not available. The use of feasible regions also narrows the potential simulation parameter set and reduces the computation load in generating simulation runs. An robust optimization problem is formulated and integrated with the model calibration. The proposed point and interval estimators of the optimal design are mathematically proved to have consistency and coverage properties.

CHAPTER I
Introduction

1.1 Motivation

Functional data analysis has been widely used in various applications such as human body kinematic pattern analysis and biomechanical injury assessment using force/movement responses, manufacturing process control based on various in situ sensing signals, weather forecasting based on continuous environmental sensing signals etc. In such cases, one of the common interests is to model the functional responses in order to characterize the system's behavior or improve the system design. For instance, in biomechanical applications, human body trajectory signals during vehicle crash tests are often used to evaluate the crash injury level, which further indicates the safety level of the vehicle. However, these functional signal responses are subject to a variety sources of uncertainties. These uncertainties can be divided into three main aspects: (1) auto-correlation between different sampling time points; (2) complicated functional or cross-correlation relationships among different sensors; (3) multiple level uncertainties caused by subject-to-subject variability, within-subject test-to-test randomness. The system performance assessment and prediction require estimating both the mean and variation of the functional signal responses to consider all above uncertainties.

Generally, limited physical tests are conducted and the estimation performance is determined by the sample size of the physical tests. However, it is often the case

that conducting physical tests are very limited due to cost or time, thus resulting in a low statistical power of the estimates. To address this issue, physical-model-based computer simulations are generated to predict the physical system behaviors. The attained reliable simulation models not only can reduce expensive subject testes but also can help fully understand the subjects induced variability for improving the product/system design.

Although computer simulations are increasingly used for improving system design, computer simulation model sometimes cannot represent the true physical responses exactly. There are two major sources of this inexactness. Generally, simulation parameters are unknown in the physical tests but influence the simulation results (such as cushion friction and cushion damping). A proper selection of simulation parameters is required before running a computer simulation model. Moreover, even if the values of simulation parameters are accurate, there may still exist a bias between simulation responses and the corresponding physical test. Both the unknown simulation model parameters and the simulation model bias introduce errors in the computer model simulation responses.

This dissertation is motivated to address the following three key research issues in uncertainty quantification for functional data in biomechanical applications:

- Confidence band construction for univariate functional signal responses based on principal component analysis.
- Confidence band development for bivariate functional signal responses using Gaussian process modeling.
- Robust system design optimization with limited experimental data and an inexact simulation model.

This dissertation mainly focuses on functional data in biomechanical applications.

The developed methodologies can be further applied or extended to various other applications where functional data analysis are desired.

1.2 Overview of dissertation

In this section, three research topics highlighted in the previous section are briefly discussed in the following subsections. For each research topic, research overviews, challenges and the proposed methodology are given.

1.2.1 Confidence band (corridor) construction for univariate functional signal responses based on principal component analysis

The fidelity of the responses of human surrogates used for injury prediction, such as crash test dummies and human finite element models, has usually been assessed by comparing surrogate responses to biomechanical response corridors. These corridors describe the population variability in a particular mechanical response (e.g., force produced by impacting a body region) measured in biomechanical tests involving human cadavers or other surrogates such as animals, volunteers etc. Such response corridors are typically developed using a process that involves (1) normalizing response data to account for subject-to-subject variability in physical characteristics, (2) aligning the data to account for phase variability in measured experimental responses, and (3) constructing a corridor based on point wise distributions of the normalized and aligned data (e.g., ± 1 standard deviation at each time point).

In biomechanical applications, vehicle crash tests are often used to obtain human body's force response signals for evaluating vehicle safety, in which human force responses are sensitively affected by human body anthropometry parameters. Therefore, the research issue is how to model the inevitable subject-to-subject variability in the biomechanical functional responses data. As an illustration, Figure 1.1 shows one of the crash test settings, in which a dummy was placed on the occupant

sled before being collided by the accelerated impact wall to simulate the side impact during a car crash. The sled tests were conducted on different dummies with different anthropometry parameters, such as stature, BMI, breast width, etc. Therefore, the development of a prediction model of human force responses should consider human body anthropometry parameters as essential covariates. Figure 1.2 illustrate the basic scheme for vehicle safety evaluation, in which functional data fitting and confidence band prediction are two key issues needed to be investigated. Based on the domain physical model, the attained confidence bands can be further converted into bone fracture levels for evaluating the safety of vehicle designs. The objective of Chapter 2 of the dissertation is to develop a systematic approach to generate corridors that consider subject-to-subject variability.

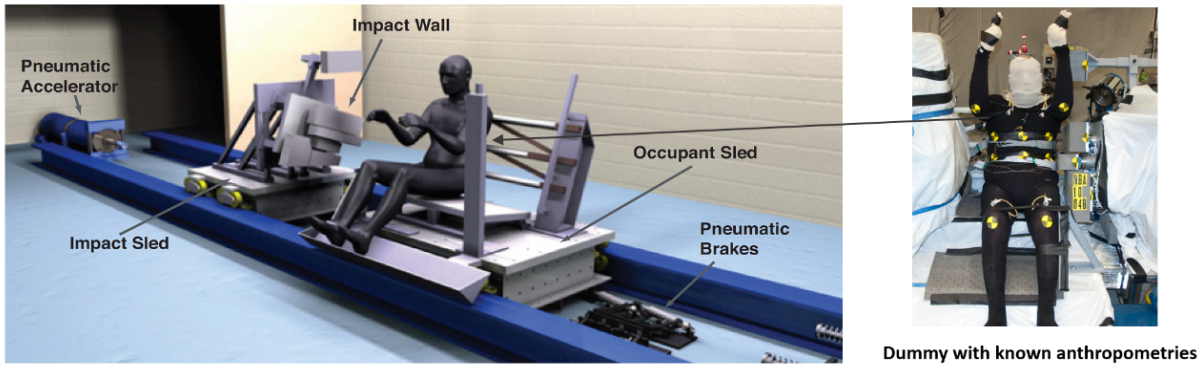

Figure 1.1: UMTRI dual-sled impact facility

Besides the naive eyeballing method (ISO) without numerical analysis, the most common approaches to response normalization include equal-stress equal-velocity normalization (Eppinger et al., 1984) and impulse-momentum normalization (Mertz, 1984b). Equal-stress equal-velocity normalization uses dimensional analysis along with the assumption that all subjects are geometrically similar to derive relationships between fundamental parameters (mass, length, time). Additional assumptions of

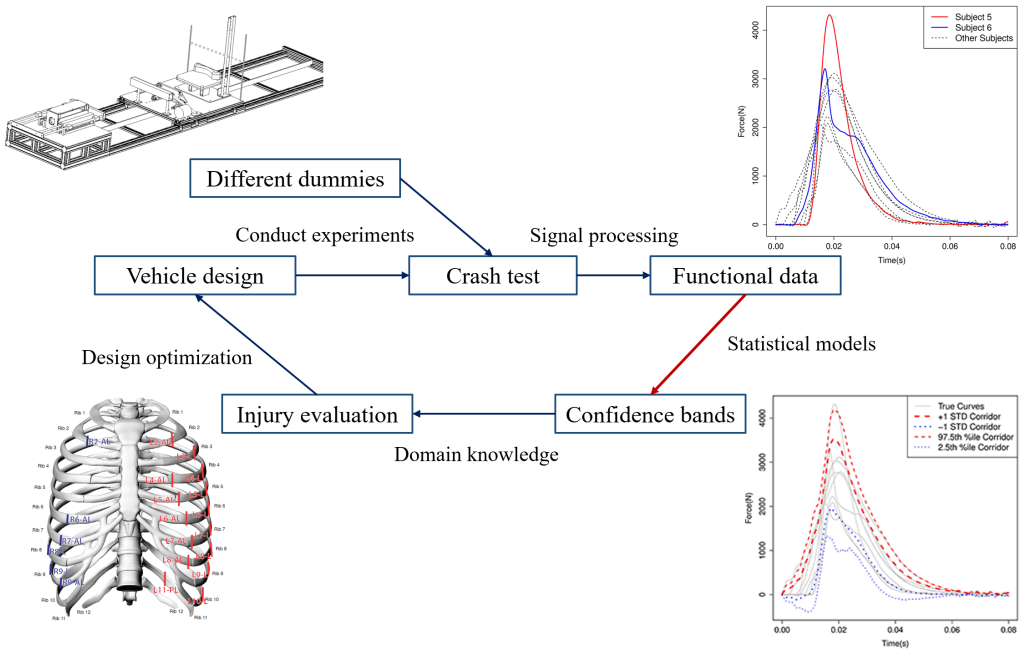

Figure 1.2: Vehicle safety evaluation scheme

equal density and modulus of elasticity among subjects allow all relationships between fundamental parameters to be normalized to a reference based solely on a ratio of subject mass to reference mass. Impulse-momentum normalization assumes that subject response is described by a simple mechanical model, usually a spring-mass system, and determines relationships between stiffness and mass of a reference and a subject. Mass relationships are typically expressed as the ratios of the experimentally determined effective mass of a body region to the average effective mass of the sampled population. Assumptions of geometric similitude and equal modulus of elasticity across a population are then commonly applied, allowing stiffness ratio to be expressed as a ratio of lengths. Later implementations of impulse-momentum normalization have used slightly more complex mechanical models and stiffness ratios determined from experimental data (Viano et al., 1989; Moorhouse et al., 2013). Another implementation is to use a deformation energy approach (Donnelly et al., 2014). However, some of these approaches assume a relationship between body char-

acteristics (also known as subject variables throughout the dissertation) and response or require information that may not be available, like deformation of a body region. Those restrictions motivate us to develop a statistical method that models the relationship between body characteristics and response signals without using any other information. A statistical method is preferred since it considers the uncertainties and can be used to generate corridor limits with different confidence levels.

Existing methods for response normalization are based on assumed relationships between a subject and a reference, such as similar geometry or that the response of a body region can be described by a simple mechanical model. In practice, these assumptions are violated to varying degrees. Subjects from the same population may not be geometrically similar, modulus varies with factors like age for different tissues, the data needed to fit mechanical models may not be available, and the validity of even simple mechanical models for a particular response is often difficult to prove with the small sample sizes typically present in experimental studies involving cadavers.

To overcome the challenges, we propose a method for generating response corridors that models the variability in univariate functional responses with anthropometric variables and uses these models along with target values for the anthropometric variables to develop a corridor. This method is implemented by the following steps: (1) aligning signals using established methods; (2) performing a principal components analysis (PCA) on the aligned data,; (3) modeling the relationships between principal component (PC) features and subject anthropometry; (4) performing Monte Carlo simulation on these models to generate sets of PC features associated with a target anthropometry; and (5) reconstructing functional responses using these PC features, and generating corridors from the reconstructed functional responses. A demonstration of this method using recently reported impact force data from lateral

impact tests on whole seated cadavers is provided, and corridors generated with and without considering the effects of subject anthropometry are compared. A comparison of corridors generated using traditional scaling techniques to corridors generated using the PCA/regression/Monte Carlo simulation approach is also provided. The details of the methodology development will be discussed in Chapter 2.

1.2.2 Confidence band development for bivariate functional signal responses using Gaussian process modeling

There are often situations where two functional responses need to be modeled simultaneously in order to understand the inherent physical dependent relationship between two signals. For example, body movement trajectories in vertical (Z) and horizontal (X) directions are of physical interest in assessing vehicle safety using the body's kinematic movement pattern. Figure 1.3 shows the experiment setup for crash tests conducted by the Children's Hospital of Philadelphia (Arbogast et al., 2009). Subjects with different subject variables are tested in the experiments multiple times. Each replicate test run is called a trial. The mechanical responses contain force, acceleration, velocity or location signals that are collected from different sensors (highlighted by the circles in Figure 1.3) in each test.

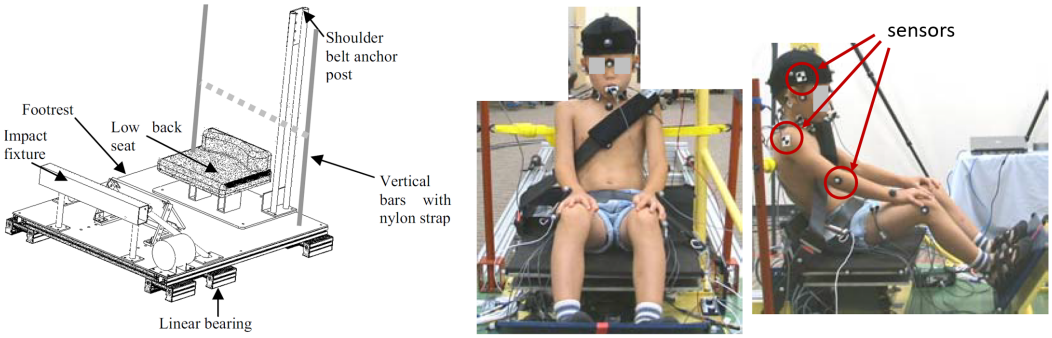

Figure 1.3: Example of crash test device

Among all the responses, the bivariate head trajectories in vertical and horizontal

directions serves as important indicator of crash impact on head (Lobdell et al., 1973). The left and middle panel in Figure 1.4 are examples of head trajectories in two directions collected from multiple identical trials on a single subject. Combining the two signals yields the bivariate trajectories in the right panel, which is often used to evaluate the head damage during crash.

There are two main challenges when building a confidence band illustrated by the shaded area in the right panel of Figure 1.4. First, it is difficult to capture the bivariate functional profile shape in the resultant confidence bands, especially when responses in different directions are not shown as a one-to-one mapping. For example, in the right panel of Figure 1.4, the dashed line shows for given $X = 300$ head trajectory in X direction, there exist two head trajectory values in Z direction. Thus the time index should be kept in the model for representing these bivariate relationships. Second, the confidence band should account for different sources of vari-

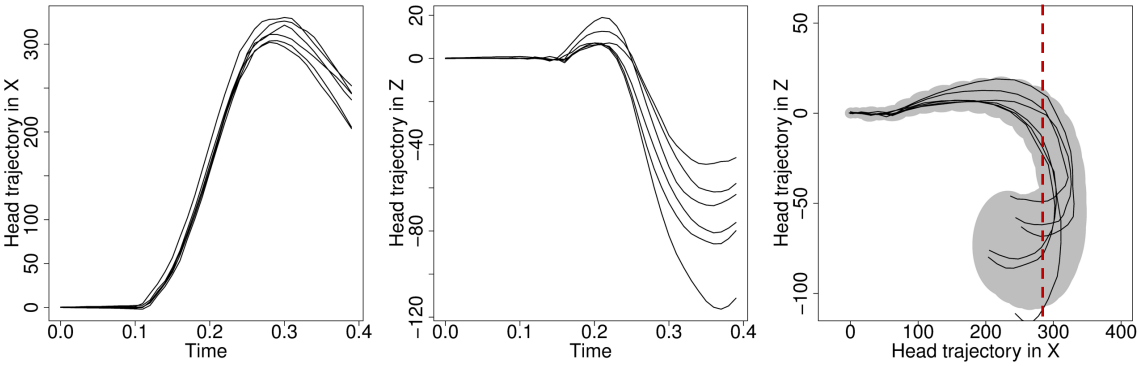

Figure 1.4: Profile signal responses and the corresponding confidence band

ations, including the subject-to-subject variations due to different subject variables, the within-subject variations that explain the differences among multiple trials, the auto-correlation among time points and the cross-correlation between the bivariate functional responses.

A variety of existing methods are developed to include subject-to-subject variations when building the confidence bands for univariate functional signals. Normalization techniques are typically used to construct confidence bands based on a physical system. Equal-stress equal-velocity normalization (Eppinger et al., 1984) and impulse-momentum normalization (Mertz, 1984b) assume that the response signals are described by a simple mechanical model, (e.g., a spring-mass system), which determines the relationships of the stiffness and mass between a reference and a subject. Donnelly et al. (2014) construct the confidence bands using a deformation energy approach. Normalization methods create the confidence bands point-wisely, which ignores the auto-correlation among time points. To address this issue, methods are developed to retain the auto-correlations using statistical dimension reduction techniques. For example, Sun et al. (2016) develops the bands by linking the principal components with subject variables.

To address the cross-correlation issue and capture the bivariate functional profile shape, an intuitive way is to model one dimension of the functional signal responses as a function of the other. It is desired to apply non-parametric modeling techniques such as kernel regression (Nadaraya, 1964; Watson, 1964) since the function is often nonlinear with an unknown functional form. However, these methods do not work when the bivariate functional relationship is not a one-to-one mapping. An alternative solution is to project the data into polar coordinates and build confidence intervals for the angle and radius. For kinematic responses, there is no explicit way to specify the origin of the polar coordinates. Therefore, modeling the functional relationship between such bivariate responses needs to include both the responses in terms of time. Gaussian process modeling (Rasmussen and Williams, 2006) provides possibilities to build such a nonlinear mapping by specifying a covariance function

that takes both the auto-correlation and cross-correlation into consideration. The computational load is not acceptable if all possible combinations of time points, dimensions and features are to be included in the prediction step. A simplified Gaussian process-based approach is established in You et al. (2017) for wind energy application. However, this method requires a physical model to capture the interactions between different wind turbines which is not available for kinematic response data in crash tests. Lastly, it is also desired that the confidence band accounts for the within-subject variations among multiple trials. Stochastic kriging approach (Ankenman et al., 2010) incorporates Gaussian process modeling within a mixed effect model. It models the within-subject variations as an $i.i.d.$ normal random variable with unknown variance for univariate responses. In our case, as the responses are functional profile data, it is required to consider the auto-correlation at within-subject level.

In this chapter, a generic method is developed to construct confidence bands for bivariate functional data. The effect of subject variables is quantified by non-parametric B-spline fitting and a polynomial regression model, which is capable of capturing non-linear dependencies between the subject variables and functional responses. Moreover, a Gaussian process model is developed to model the complicated covariance structure, which can fully consider between-subjects and within-subject variability, auto-correlation between time points and cross-correlation between two responses. Therefore, the constructed confidence bands can effectively capture the bivariate functional profile shape and functional variation patterns. As a byproduct, the developed model is effectively used for testing outliers of abnormal functional responses based on the property of the developed Gaussian process model. The details of the methodology development will be discussed in Chapter 3.

1.2.3 Robust system design optimization with limited experimental data and an inexact simulation model

Computer simulations are increasingly used for predicting physical systems where physical experimental results are expensive to obtain. For example, computer simulations of vehicle crashes provide a means to investigate the effects of vehicle designs on the injury risks during car crash (Hu et al., 2015, 2013; Wu et al., 2012). Anthropomorphic test devices are used for evaluating the crash impact on injuries in different vehicle designs, which can be varied by changing belt anchorage locations, buckle locations or the types of dynamic locking tongue, etc. (see the left panel of Figure 1.5). Computer simulation parameters including seat friction, cushion softness and initial belt strain are required in the computer model in addition to the vehicle designs (shown in Figure 1.5 middle). Previous works such as Hu et al. (2015) fix computer simulation parameters at empirical values and search for the optimal vehicle design based on the generated computer simulations.

However, computer simulation models are not always exact, meaning the simulated responses cannot perfectly match with the real physical responses in the physical test (shown in Figure 1.5 right). There are two major sources of this inexactness. One is simulation parameters, some of which are often unknown in the physical tests but influence the simulation results. A proper guess of simulation parameters is required before running a computer model. The other source is, even if the values of simulation parameters are accurate, there may exist a bias between simulation responses and the corresponding physical test. Both the unknown simulation model parameters and the simulation model bias introduce uncertainty to the computer model. Our objective is to search for optimal design solutions under such uncertainty.

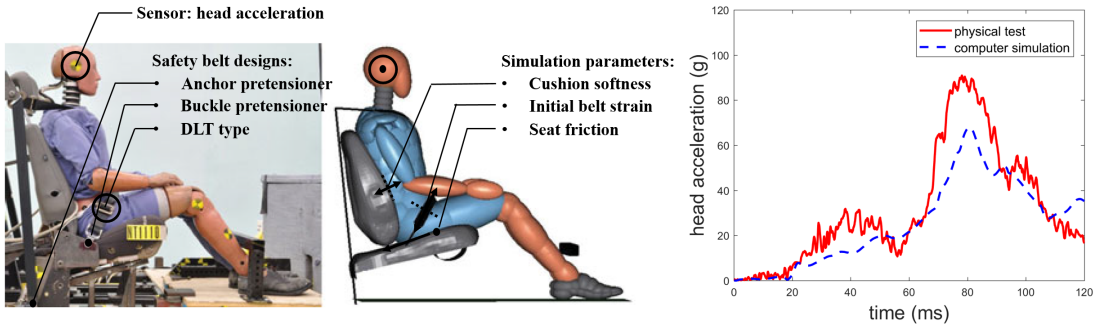

Figure 1.5: Left panel: example of a crash test study with a midsize male ATD (Hu et al., 2013). Middle panel: the computer simulation setting with a midsize male. Right panel: a comparison between the physical test response and the simulation response

Accomplishing the above objective often involves two steps: (1) model and estimate the uncertainty (2) formulate and solve an optimization problem considering the uncertainty. In the first step, different sources of uncertainty might be included such as the code uncertainty caused by the simulation model's randomness, the residual variability inherent in the physical process and the model inadequacy and parameter uncertainty generated from inexact simulation models. In this paper, we focus on deterministic but inexact computer simulation models which cannot accurately predict deterministic physical processes. For inexact computer simulation models, the simulation models should be calibrated to account for the parameter uncertainty and the model bias before being used for design optimization. Kennedy and O'Hagan (2001) proposed a Bayesian approach to model and estimate the two terms. Higdon et al. (2008) and Bayarri et al. (2007) extended the calibration approach to signal profile responses. However, it has been widely discussed (Farah et al., 2014; Gramacy et al., 2015) that the bias term between simulation and actual responses is coupled with unknown simulation parameters, which leads to a statistically unidentifiable challenge. The prevalently used Bayesian framework in Kennedy and O'Hagan (2001) estimate the simulation parameters and bias simultaneously based on specific joint

priors, which makes the posterior estimations rely on the prior assumption. Tuo et al. (2015) defined and estimated the simulation parameters as the minimizer of the $L2$ loss between the actual responses and the simulations. Plumlee (2017) extended the $L2$ loss with $L_{W_k^2(\mu)}$ loss to add weights to different regions. In these existing works, the simulation parameters are assumed to be constants of physical meanings, or deterministic functions of given experimental settings (Plumlee et al., 2016) and then estimated under specific definitions. In this way, if the optimal system design solution is searched based on the simulation responses corresponding to the estimated simulation parameters, its value will rely on the definition of simulation parameters, which cannot provide a generic guidance for system improvement. Moreover, in some of the engineering applications, the simulation parameters could be random variables that are affected by unobserved covariates, making the existing methods not applicable. Fortunately, when the objective is optimal design, the values of simulation parameters are not the main interest. A set of simulation parameters that generate reasonable simulation responses comparing to the physical tests are acceptable. In this paper, an insensitive optimal system design solution will be defined and estimated among a set of simulation parameters.

Suppose an uncertainty model can be established considering different simulation parameters and model inadequacies under the proposed computer model calibration framework, next, an optimization problem is to be formulated and solved to account for uncertainty. There exist two main approaches to formulate such a problem: reliability-based optimization and robust design optimization (Schuëller and Jensen, 2008). The reliability-based optimization approach (Valdebenito and Schuëller, 2010) has emerged to properly deal with the safety-under-uncertainty part of the problem. When formulating a reliability-based optimization problem, reliability is introduced

by setting constraints on either the failure probability (Kinser and Moses, 1967) or the pre-defined cost function (Vanmarcke, 1973) related to the responses. The one that is not used as the constraint is selected as the objective function. The formulated reliability-based optimization problem is a double-loop problem (Enevoldsen and Sørensen, 1994; Chen et al., 1997) where the reliability evaluation procedure is nested within the optimization loop. Therefore it requires additional efforts to reduce computational load by simplifying the problem. Another approach is robust optimization. It aims to search for designs that are less variant to the uncertainty effects (Bektas et al., 2017). Robust measures are chosen to be objective functions to reduce the variances of the resultant designs. Various robust measures are defined to account for the uncertainty effects. Possible robust measures include signal-to-noise measures used in the Taguchi method (Taguchi, 1986), expectancy and dispersion measures suggested in Doltsinis and Kang (2004); Jensen (2006); Lee and Park (2001) and worst-cases defined in minimax robust optimization in (Verdu and Poor, 1984). In the vehicle design applications, the reliability-based optimization cannot be formulated without a threshold that separates the safe and unsafe scenarios based on the domain knowledge. Therefore, the minimax robust optimization via evaluating the worst-cases is integrated with the proposed computer model calibration technique.

To overcome the research challenges, a method for design optimization that considers both sources of uncertainty from parameters and model inexactness is proposed. The proposed method involves two steps: (1) computing feasible regions for the computer simulation parameters and model bias; and (2) searching for optimal design solutions under a robust optimization formulation. A numerical illustration is provided for methodology illustration, followed by a case study for vehicle restraint components design optimization. The details of the methodology will be discussed

in Chapter 4.

1.3 Outline of dissertation

In this dissertation, general methodologies are developed to quantify the uncertainties of functional data for the purpose of vehicle safety evaluation and design optimization in biomechanical applications. These methodologies are validated via both simulation studies and case studies. The organization of the dissertation associated with the methodology development is shown in Figure 1.6

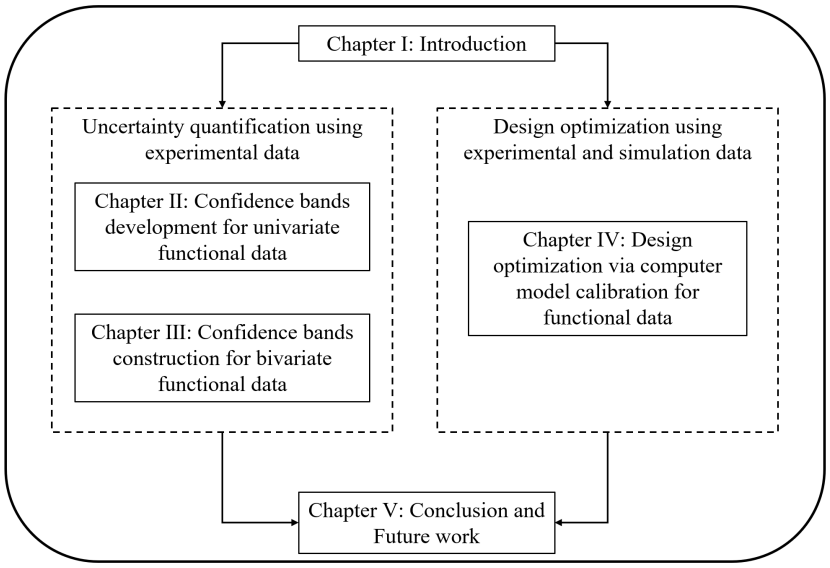

Figure 1.6: Outline of dissertation

Chapter I presents the three key research topics to be discussed in the dissertation. The motivations and challenges are also presented respectively.

Chapter II presents a new method for developing confidence bands for univariate functional signal responses by using principle component analysis considering the subjects' effects as covariates. The resultant confidence bands are narrower than those generated by existing techniques while keeping a high coverage rate of sampled functional signals.

Chapter III Shows a novel approach to construct confidence bands for bivariate functional signal responses, which integrates Gaussian process modeling for cross- and auto- correlations of bivariate functional data with the semiparametric modeling of subjects' effects on the mean of responses. The complicated covariance structure is clearly modeled and estimated in order to generate confidence bands that captures bivariate functional profile shape.

Chapter IV provides a method to search for the optimal system design using an inexact computer simulation model with uncertainty quantification. The uncertainty is quantified by specifying feasible regions instead of building a full probabilistic model, which makes the proposed method applicable when an emulator is not available. The use of feasible regions also narrows the potential simulation parameter set and reduces the computation load in generating simulation runs. A robust optimization problem is formulated and integrated with the model calibration. The proposed point and interval estimators of the optimal design are mathematically proved to have consistency and coverage properties.

Chapter V summarizes the major work and contributions of the dissertation. Some examples of future research topics are discussed.

CHAPTER II

Confidence Band Construction for Univariate Functional Signal Responses based on Principal Component Analysis

The objective of this chapter is to develop a method for generating confidence bands that model the variability in univariate functional responses considering the effect of subjects' variables. Section 2.1 elaborates the methodology for constructing confidence bands based on principal component analysis considering subjects' effects as covariates using regression analysis. Section 2.2 shows the analysis results. Section 2.3 summarizes the chapter with a discussion.

2.1 Corridor development methods

Based on the problem described in Subsection 1.2.1, the methodology development includes the following four steps. (1) aligning signals using established methods; (2) performing a principal components analysis (PCA) on the aligned data,; (3) modeling the relationships between principal component (PC) features and subject anthropometry; (4) performing Monte Carlo simulation on these models to generate sets of PC features associated with a target anthropometry; and (5) reconstructing functional responses using these PC features, and generating corridors from the reconstructed functional responses. The details of each step will be described in the following subsections.

2.1.1 Align data

As a first step, signals from different subjects are shifted in the time domain to align overall phase response. The most common approach, and the approach used in this chapter is to find the time shift that maximizes the alignment of the $i-$th subject relative to the reference subject using a similarity metric (Ripley, 2002). In the chapter, n subjects' response signals are represented as a matrix $F_{n\times p} = [f_1, ..., f_n]^T$ and its vector $f_i \in \mathbb{R}^{p\times 1}$ denotes the signal from subject i signal with p sampling points. The cross-correlation coefficient between subject $i(i \neq 1)$ and the reference subject 1 is calculated as:

$$r_{i1}(\tau) = \frac{\sum_j (f_1(j) - \mu_1^f)(f_i(j+\tau) - \mu_i^f)}{\sqrt{\sum_j (f_1(j) - \mu_1^f)^2}\sqrt{\sum_j (f_i(j) - \mu_i^f)^2}},$$

where μ_i^f is the average over all sampling points of subject's signal f_i, and τ is the shifted time to align subject i to subject 1. The optimal shifted time τ_i^* for subject i maximizes its cross-correlation coefficient, i.e.,

$$\tau_i^* = \arg\max_{\tau} \{r_{i1}(\tau)\}.$$

By following the same procedure to align all other subjects with subject 1, the aligned signals are represented as a matrix $Y_{n\times p} = [y_1...y_i...y_n]$, where $y_i(j) = f_i(j + \tau_j^*), j = 1, ..., p$. Let $\bar{y} = \frac{1}{n}\sum_{i=1}^n y_i$ represent the average signal of n aligned subjects, and $x_i = y_i - \bar{y}$ denote the deviation of subject i's signal from the average signal. Then, the matrix $X_{n\times p} = [x_1...x_i...x_n]^T$ represents all n subjects' deviation from the mean response.

2.1.2 Principal component analysis

Principal component analysis (PCA) is used as an orthogonal linear transformation to obtain a reduced dimension of features that can describe the original subject

signals accurately and efficiently. The linear transformation is formed by a set of eigenvectors $u_k = [u_{k1}...u_{kp}] \in \mathbb{R}^{p\times 1}, (k = 1, ..., q; q \leq p)$ sorted based on the descending order of eigenvalues λ_k, which are obtained via the singular value decomposition (SVD) of the sample covariance matrix $X^T X$. Here, SVD is used since the sample size is rather small. By projecting x_i on the $k-$th eigenvector, a PC feature (also commonly called a PC score), $z_{ik} = x_i^T u_k$ is obtained. In this chapter, z_{ik} is called a PC feature whose variance is equal to eigenvalue λ_k. If q eigenvectors are applied on x_i, we can obtain q PC features for subject i, denoted as $z_i = [z_{i1}...z_{ik}...z_{iq}]^T \in \mathbb{R}^{q\times 1}$. The percentage of the variance represented by these q PC features is denoted as C_q, which is calculated as follows:

$$C_q = \frac{\sum_{k=1}^{q} \lambda_k}{\sum_{k=1}^{p} \lambda_k} \times 100\%. \tag{2.1}$$

By setting a threshold η on C_q, i.e., $C_q > \eta\%$, we can determine the minimum q, which decides how many PC features are essentially needed to represent $\eta\%$ of the total variance of the original signals.

To see how well q PC features represent original signals, each signal can be reconstructed in the time domain and compared to the corresponding aligned original signal. For subject i, the approximated signals based on these q PC features are reconstructed by:

$$\hat{y}_i = \sum_{k=1}^{q} \hat{x}_i(k) + \bar{y}.$$

where $\hat{x}_i(k) = z_{ik}^T u_k$ indicates the contribution of the $k-$th PC feature z_{ik} to the approximation signal $\hat{y}_i$ in the time domain. The variance of approximation errors by using these q PC features is $\mathbb{E}[\hat{y}_i - y_i]^2 = \sum_{k=q+1}^{p} \lambda_k$, which is limited to $(1 - \eta\%)$ of the total variance of the original signals.

2.1.3 Stepwise regression

To further analyze the effects of subject anthropometry, a stepwise regression approach is used to model the relationships between q PC features and subject anthropometry measurements. Because the PCA transform is an orthogonal linear transform, the resulting PC features are mutually independent. As a result, individual regression models can be built for q PC features separately. To analyze the effect of anthropometry variables on the $k-$th PC feature, the regression model is written as:

$$z_{ik} = \sum_{j=1}^{r} w_{ij}\beta_{kj} + \varepsilon_{ki}, k = 1, ..., q, \tag{2.2}$$

where $w_{ij}(i = 1, ..., n; j = 1, ..., r)$ represents the $j-$th anthropometry variable measurement of subject i, i.e., matrix $W = \{w_{ij}\} \in \mathbb{R}^{n\times r}$ represents all anthropometry measurements of n subjects with r attributes. $\beta_{kj}(j = 1, ..., r; k = 1, ..., q)$ is the regression model coefficient representing the anthropometry measurement j's contribution to the $k-$th PC feature. $\varepsilon_{ki}(i = 1, ..., n; k = 1, ..., q)$ is the normally distributed residual error with mean 0 and variance ξ_k^2.

2.1.4 Construct corridor limits

To assess the effect of considering subject anthropometry on corridors, corridor bounds were generated with and without the use of regression models. The detailed procedures of each approach are discussed in the following two subsections.

Construct corridor limits without using regression models

To construct corridor limits without considering the effects of subject anthropometry, we assume all the subjects' responses are from the same probability distribution and leverage the normal distribution of PC features. The normality assumption can be validated via the QQ-plot of the PC features. The steps for constructing the

corridor limits using q PC features are:

Step 1 For the $k-$th PC feature ($k = 1, ..., q$), z_{ik}, calculate its sample mean and sample variance over n tested subjects as: $\hat{\mu}_k = \frac{1}{n}\sum_{i=1}^{n} z_{ik}$;$\hat{\sigma}^2 = \frac{1}{n-1}\sum_{i=1}^{n}(z_{ik} - \hat{\mu}_k)^2$.

Step 2 Based on above estimated mean and variance, apply the normal distribution of $z_{ik} \sim N(\hat{\mu}_k, \hat{\sigma}_k^2)$ to perform a Monte Carlo simulation, which generates N samples (a large integer number) for the $k-$th ($k = 1, , q$) PC feature, i.e., $\tilde{z}(k) = \{\tilde{z}_{ik}\}, i = 1, 2, ..., N$. The notation of "$\sim$" in the chapter denotes the simulated PC features or the surrogate signals used in (2.3) below.

Repeat step 1 and step 2 for all q PC features.

Step 3 Based on (2.3), construct N surrogate signals by using all generated q PC features of $\tilde{z}_{ik}(i = 1, ..., N; k = 1, ..., q)$:

$$\tilde{y}_i = \sum_{k=1}^{q} \tilde{z}_{ik} u_k + \bar{y}. \tag{2.3}$$

The row vector of $\tilde{y}_i^T (i = 1, ..., N)$ represents subject i's signal, based on which the matrix $\tilde{Y}_{N\times p}$ is formed to represent all N surrogate signals. Each column vector of $\tilde{Y}_{N\times p}$ is denoted as $\tilde{y}(j)(j = 1, ..., p)$, which represents the $j-$th sampling data of all the surrogate N signals.

Step 4 Calculate the corridor limits by using the pointwise quantile of the surrogate signals on each sampling data point $j, (j = 1, , p)$:

$$CL_j = q_{1-\alpha/2}(\tilde{y}(j)), LCL_j = q_{\alpha/2}(\tilde{y}(j)), \tag{2.4}$$

where function $q_\tau(\nu)$ represents the $\tau-$th quantile of random variable ν.

Construct the corridor limits by incorporating regression models

If subject anthropometry variables are significant predictors of PC features then narrower corridor limits can be generated for a particular set of anthropometry mea-

surements (see comparisons in subsection 2.2.4). The steps for developing corridor limits that consider subject variables are:

Step 1 Apply PCA, calculate the $k-$th $(k = 1, , q)$ PC feature z_{ik} for each subject $i, (i = 1, , n)$ by projecting signal x_i on the $k-$th eigenvector u_k. q is so determined that $C_q < \eta\%$ is satisfied under a given threshold $\eta\%$, where C_q is defined in (2.1).

Step 2 Based on (2.2), run stepwise regression for each PC feature with r anthropometry measurements as the independent variables. Specifically, the feedforward variable selection approach is taken to sequentially select the critical anthropometric measurements for each PC feature. The estimated regression coefficients and the corresponding standard errors are denoted as $\hat{\beta}_{kj}(j = 1, ..., r)$ and $\hat{\xi}_k$, respectively. The expected prediction of the $k-$th PC feature is calculated by $\hat{\mu}_k^r = \sum_{j=1}^{r} w_{ij}\hat{\beta}_{kj}$.

Step 3 Simulate N samples for the $k-$th PC feature (denoted as $\tilde{z}_{ik}$) based on the normal distribution $N\left(\hat{\mu}_k^r, \hat{\xi}_k^2\right)$.

Step 4 Reconstruct N simulation curves according to (2.3).

Step 5 Calculate the pointwise quantile according to (2.4).

2.2 Case study and analysis results

2.2.1 Data source

As a demonstration, the methods described above were applied to pelvis impact force data collected in a recent study in which the lateral aspects of nine seated post-mortem human subjects (PMHS) were impacted with a segmented wall in a manner that reproduced important aspects of the loading of the body in a side impact crash (Wood et al., 2014). Each of the impact segments was instrumented

to record applied force. The body dimensions of the PMHS used in this study were characterized using standard methods. Anthropometric measurements considered in the regression analysis are listed in Table 2.1.

Table 2.1: Available Anthropometric Measurements

Subject Index	1	2	3	4	5	6	7	8	9
BMI (kg/m2)	27.59	13.98	16.49	17.04	20.55	25.51	26.91	24.07	26.74
Stature(cm)	157	167	163	168	160	160	160	180	172
Mass (kg)	68	39	43.8	48.1	52.6	65.3	68.9	78	79.1
Vertex to Symphysis (cm)	84	86	86	81	85	86	79	81	80
Waist Height (cm)	74	101	86	103	93.5	99	91.5	100	106
Tibiale Height (cm)	44	48	48	50	47.5	31	41.5	45	51
Shoulder Breadth (cm)	37	37	36.9	37.7	40.1	39	40	43	39.2
Waist Breadth (cm)	38	23	25.3	27.5	29.9	33	35.5	35.5	36.8
Hip Breadth (cm)	39	33	31.5	32	32	35.5	36	34.6	38.7
Forearm Hand Length (cm)	26	23	39	40	46.5	46	39.5	44	50
Waist Depth (cm)	20	18	17.4	16.6	15.4	18.5	21.5	25	19
Effective Pelvis Mass (kg)	25.3	11.9	10.1	9.9	16.6	18.6	19.2	21.2	18.7

The aligned pelvis force signals of nine subjects are shown in Figure 2.1. Each force signal is represented as a $800-$length time series. The common pattern shared by nine signals is that the signal starts from zero and increases to its central peak, and thereafter decreases to zero at the end. In contrast, the signal for Subject 5 shows a significant central peak whose maximum is over $4kN$, which is much higher than the other signals, and the signal for Subject 6 has a "shoulder" shape within the sampling period from $20ms$ to $30ms$.

2.2.2 PCA

PCA was conducted on the nine subjects' signals. The resulting contribution of each PC to the cumulative variance, C_q, is shown in Figure 2.2. The required number of PCs decided by the pre-set threshold of $\eta = 99\%$ was reached by the $5-$th PC ($q = 5$). Limiting the number of PCs simplifies the corridor generation process, especially when responses from more subjects are added. The resultant PC scores are shown in Table 2.2. For new observations to be added to the study, if we were

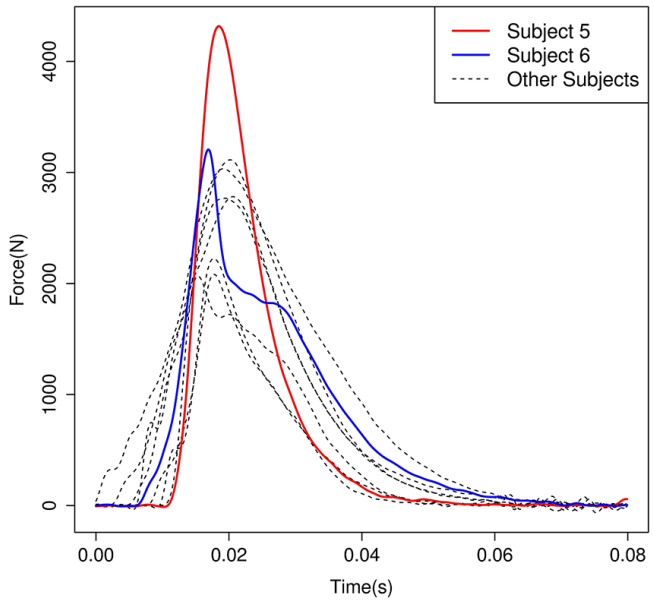

Figure 2.1: Aligned signals

comparing a new response to the distributions of previous responses, i.e. detecting outliers, new observations would be directly projected into the PC space by using the eigenvectors calculated from existing observations. If we were to develop a new corridor by combining all the data, we would re-run the PCA.

Table 2.2: PC Scores

PC Scores	PC1	PC2	PC3	PC4	PC5
Subject 1	-10317	3993	335	-2254	-1344
Subject 2	7731	2750	1349	2055	-1811
Subject 3	10317	725	-1223	-1424	215
Subject 4	10086	-674	-1165	-1216	442
Subject 5	-2816	-12591	1010	-18	-428
Subject 6	-1064	2702	5043	11	-132
Subject 7	-3553	1665	-2142	1332	406
Subject 8	-7142	710	-1948	662	258
Subject 9	-3243	720	-1258	852	941
Mean	0	0	0	0	0
STD	7563	4926	2269	1403	1023

To interpret the PCA results, the contribution of the first PC feature is visualized in Figure 2.3(a) and Figure 2.3(d). The reconstructed signal by the first PC feature, i.e., $\hat{x}_i(1) = z_{i1}^T u_1$, is shown in Figure 2.3(a), and Figure 2.3(d) shows $\hat{x}_i(1) + \bar{y}$. The

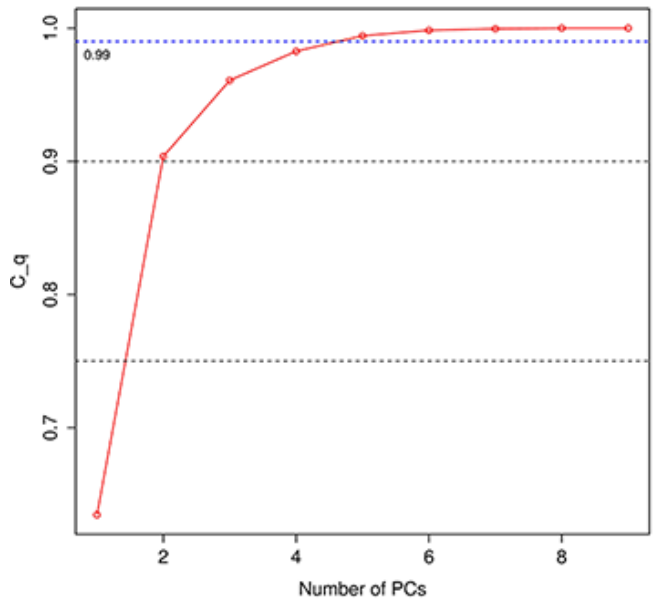

Figure 2.2: Cumulative variance contribution of PCs

first PC feature can be interpreted as the representation of the overall profile shape variations among nine subjects.

Similarly, the contribution of the second PC feature, i.e., $\hat{x}_i(2) = z_{i2}^T u_2 (i = 1, ..., 9)$ is visualized in Figure 2.3(b), which shows Subject 5 is quite different from other subjects especially around the central peak area. To further interpret the second PC feature, Figure 2.3(e) compared the reconstructed Subject 5's signal by using the first two PC features plus the average signal, i.e., $\hat{x}_5(1) + \hat{x}_5(2) + \bar{y}$ with that by only using the first PC feature plus the average signal, i.e., $\hat{x}_5(1) + \bar{y}$. Based on the comparison in (e), the second PC feature mainly contributes to signal variation around the central peak area. In this test dataset, subject 5 shows an excessive difference around the central peak area from other 8 subjects.

The similar analysis is conducted for the third PC feature. Figure 2.3(c) shows the reconstructed signal $\hat{x}_i(3) = z_{i3}^T u_3$ by only using the third PC feature, which indicates Subject 6 is significantly different from other subjects. To obtain a better

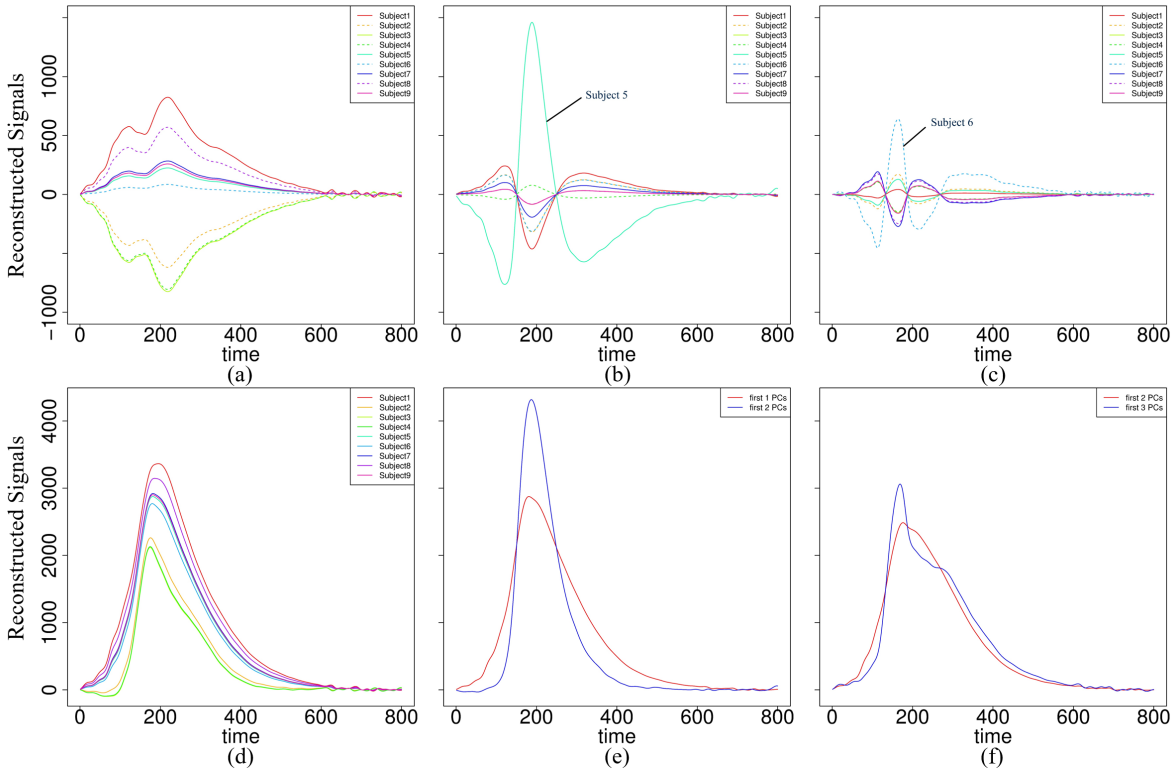

Figure 2.3: (a) The first PC's contribution for all subjects; (b) The second PC's contribution for all subjects; (c) The third PC's contribution for all subjects; (d) The reconstructed signals from PC1 for all subjects; (e) The reconstructed signal from PC1 and that from PC1-PC2 for Subject 5; (f) The reconstructed signal from PC1-PC2 and that from PC1-PC3 for Subject 6

comprehension of the third PC feature, Figure 2.3(f) compares the reconstructed signal of $\sum_{k=1}^{3} \hat{x}_6(k) + \bar{y}$ by using the first 3 PC feature plus the average signals with that of $\sum_{k=1}^{2} \hat{x}_6(k) + \bar{y}$ by using the first 2 PC feature plus the average signals. Figure 2.3(f) reveals a unique "shoulder shape" that is mainly contributed by the third PC feature, which results in the difference between Subject 6 and other subjects in Figure 2.3(e).

2.2.3 Regression analysis on anthropometry variables

The anthropometry variables may be highly linear correlated, giving unreliable regression models. Therefore, one variable is removed from each pair of highly correlated variables (over 0.6 linear correlation coefficients) prior to the regression analysis. To characterize the relationship between the impact force signals and the subject anthropometry variables listed in Table 2.2, regression models were built for the first five PC features. Instead of arbitrarily picking anthropometry measurements, a stepwise linear regression was used to determine which variables are significant to be included in the model. At each step, the variable leading to the largest adjusted R^2 was kept until a maximum of three anthropometric variables were selected. The number of anthropometric variables used in the regression was limited to three to avoid over fitting considering a relatively high dimension of anthropometry measurements ($r = 11$) compared to a fewer number of tested subjects ($n = 9$). If more subjects were added, more variables could be used in the regression equations.

Table 2.3 presents the selected anthropometric measurements and their corresponding estimated coefficients, where R^2 and adjusted R^2 (denoted as R^2_{adj}) are used to indicate the regression fitting performance. For the first and the third PC features, both R^2 and R^2_{adj} are much higher than that of other PCs, suggesting an adequate model for predicting these two PC features based on the selected dimensions.

For PC 1, higher waist breadth was associated with higher pelvis force ($p < 0.05$) and vertex to symphysis and tibiale height were significantly associated with the third PC. The "shoulder" shape shown in Figure 2.1 was associated with the third PC score and with larger vertex to symphysis distance and smaller tibiale height. In contrast, no variable was significantly associated with PC 2, which is related to the peak at $20ms$. As a result of this and because the PC score of Subject 5 was an extreme of the distribution in scores of PC 2, the PCA and regression method generates a corridor that does not include the peak in the response for Subject 5, as shown in Figure 2.4 and discussed below.

Table 2.3: Stepwise Regression Model and The Selected Anthropometry Measurements (standard deviations are in parentheses. "*" or "**" denotes variables with p-values smaller than 0.05.)

Responses	β_{k0}	β_{k1}	β_{k2}	β_{k3}	R^2	R^2_{adj}
PC1	Intercept	Waist Breadth	Vertex to Symphysis	Shoulder Breadth	0.9033	0.8452
	157575.9*	-1375.2**	-968.8	-861.6		
	(53744.2)	(245.0)	(478.7)	(620.0)		
PC2	Intercept	Waist Breadth	Vertex to Symphysis	Shoulder Breadth	0.4839	0.1743
	34823.4	-2077.1	843.5	234.6		
	(27581.6)	(1063.6)	(570.3)	(273.6)		
PC3	Intercept	Waist Breadth	Vertex to Symphysis	Shoulder Breadth	0.8241	0.7186
	-42041.28	536.30*	-202.10*	68.91		
	(16682.13)	(168.29)	(73.07)	(44.81)		
PC4	Intercept	Waist Breadth	Vertex to Symphysis	Shoulder Breadth	0.4612	0.1379
	-9876.52	94.79	202.80	-42.38		
	(11532.27)	(60.51)	(272.58)	(91.92)		
PC5	Intercept	Waist Breadth	Vertex to Symphysis	Shoulder Breadth	0.6981	0.517
	45868.68	226.04*	-851.99*	-770.03		
	(18921.17)	(75.45)	(303.62)	(346.66)		

2.2.4 Corridor bounds with and without considering subject anthropometry

Figure 2.4 illustrates corridor limits representing the 2.5−th and 97.5−th quantiles (i.e., spanning the central 95%) and plus-minus-one standard deviation of the data, generated by Monte-Carlo simulations based on the estimated distributions of 5 PC features without considering subject anthropometry. Figure 2.4(a) shows the 1000 simulated signals and the associated corridor limits (dashed line). Figure 2.4(b)

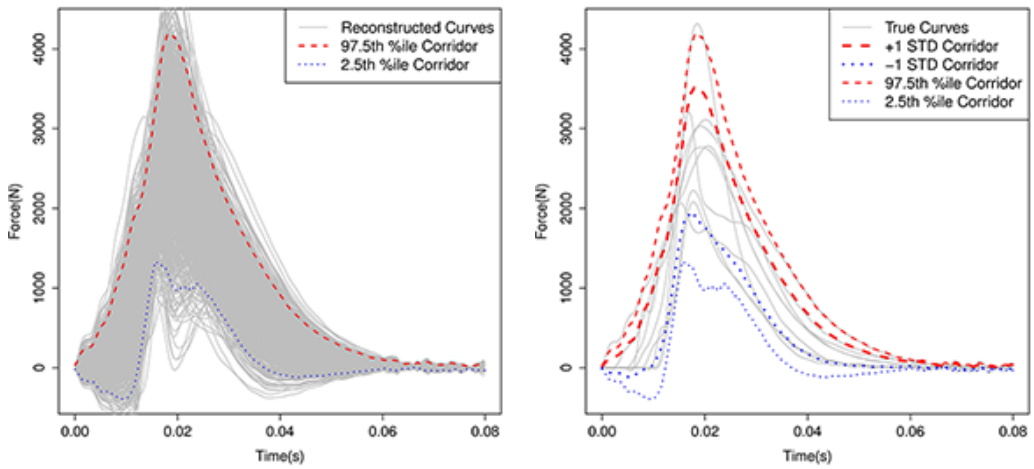

Figure 2.4: (a) Corridor limits with simulated signals; (b) Corridor limits with original signals.

shows the comparison between the estimated corridor limits (dashed lines) and the original signals (solid lines). The estimated corridor limits cover the original signals except a small portion of the signal from Subject 5 at the central peak area.

Figure 2.5 compares corridor bounds constructed using the PCA/regression/Monte Carlo simulation approach with significant predictors of PC features shown in Table 2.1 for pelvis force responses from Subject 5 (Figure 2.5(a)), Subject 6 (Figure 2.5(b)), and Subject 7 (Figure 2.5(c)). These subjects had responses that were typical, had a relatively high peak at $\sim 20ms$ or had a shoulder shape. Because the responses are significantly associated with body dimensions, corridor limits constructed using the regression models can better reflect the shape of subject responses than those developed without using the regression models. The "narrower corridor" reflects a smaller variance under the same confidence level. However, a smaller variance does not necessarily generate a better corridor if it fails to reflect the signal profile shape due to a substantial bias error.

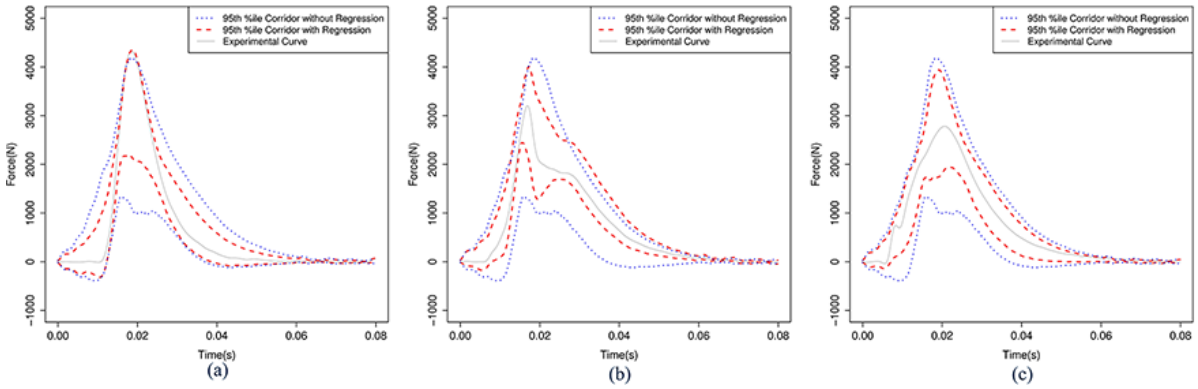

Figure 2.5: (a) Effect of using regression models to construct corridor limits for subjects whose body dimensions are similar to Subject 5; (b) Effect of using regression models to construct corridor limits for subjects whose body dimensions are similar to Subject 6; (c) Effect of using regression models to construct corridor limits for subjects whose body dimensions are similar to Subject 7.

2.2.5 Comparison with corridor bounds generated by scaling techniques

As indicated above, scaling techniques, such as equal-stress, equal velocity scaling (Eppinger et al., 1984) or impulse-momentum scaling (Mertz, 1984a) based on dimensional analysis or assumed mechanical models are commonly used to either normalize responses to account for variability in body size or to scale a corridor from one reference size to another (e.g., scaling a corridor that represents a midsize male response to a corridor that represents a the response of a small female). In contrast, the approach developed in this manuscript is based entirely on relationships between signal responses and anthropometry variables that exist in the experimental dataset.

Figure 2.6 compares corridors generated by the PCA/regression/Monte Carlo simulation approach with the body dimensions from Subjects 5, 6, and 7 to corridors generated using equal-stress equal velocity scaling based on whole-body mass and impulse-momentum scaling based on hip breadth and the effective mass of the pelvis. Table 2.1 provides the subject characteristics and effective masses used in the scaling processes. In each case, the PCA/regression/Monte Carlo approach results in corri-

dor limits that are narrower and can better reflect the shape of the original signal. As shown in Figure 2.6(b), PCA/regression/Monte Carlo captures shoulder shape from Subject 6, while the other methods do not. Figure 2.6(c) shows that although Subject 5's high central peak is not covered by any of the estimated corridor limits, PCA/regression/Monte Carlo better captures the peak shape than the traditional scaling methods.

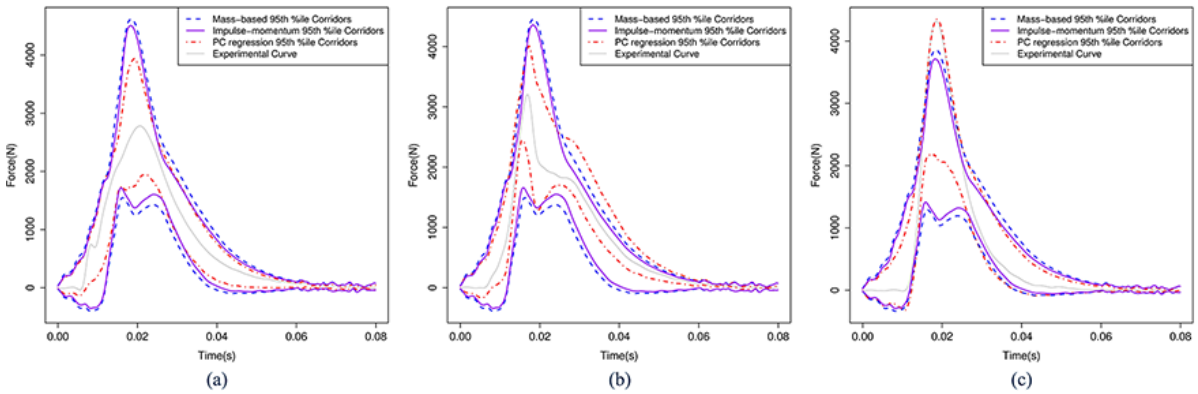

Figure 2.6: (a) Comparison between different corridor construction methods for Subject 7; (b) Comparison between different corridor construction methods for Subject 6; (c) Comparison between different corridor construction methods for Subject 5.

2.3 Discussion

The PCA, regression, and Monte Carlo simulation approach to corridor development is a departure from traditional techniques for response corridor development that involve normalizing and scaling experimental responses to a particular reference size (e.g., the small female). In particular, the PCA, regression, and Monte Carlo is based entirely on empirical data than either dimensional analysis and/or assumed relationships between size and response described by simple mechanical models. Because of this difference, the PCA, regression, and Monte Carlo approach should result in corridors that more accurately describe the target response as long as there are

sufficient experimental data that can be used in corridor development. If sufficient data do not exist, then scaling approaches to corridor development, and in particular newer scaling approaches like those proposed by Moorhouse et al. (2013) and Donnelly et al. (2014), may offer improved performance, provided that the deformation data required by these approaches are available.

The method described in this chapter aligns data in the time domain to an arbitrarily selected reference response prior to performing PCA, similar to the alignment approach proposed by Maltese et al. (2002). However, such an approach can bias results if a reference response does not represent the average response. Alternative approaches that address this issue by aligning all signals to the mean signal or segments of a mean signal have been proposed (Donnelly and Moorhouse, 2012; Nusholtz et al., 2013; Gayzik et al., 2015). These methods can be implemented with the PCA, regression, and Monte Carlo simulation approach described in this chapter without any loss of generality. When implementing any alignment method, the relationship between the phase shift produced by the alignment and subject body dimensions should be explored. If such relationships exist, then consideration should be given to statistically modeling them and implementing the resulting statistical models as phase shifts on the corridor developed following Monte Carlo simulation. Another alternative approach is to perform the analyses in the spectral domain with a windowed transform of the sensor data which should be insensitive to the location of the rise and peaks in the time domain.

The proposed method is applicable when signals have similar shape and are well aligned. Also, the PCA method works well when signals are smooth. Otherwise other techniques such as wavelets or Fourier transformation are suggested. For example, the Discrete Fourier Transform represents the signals as a combination of

sine/cosine functions with a range of frequencies. However, PCA is more efficient than alternative methods in which the basis functions are predefined, allowing the signals to be represented at a given level of fit with fewer coefficients, simplifying the regression step.

Similar to other current methods for corridor development, the PCA, regression, and Monte Carlo simulation method can generate corridors that encompass responses that are physically unrealistic, such as the negative force-values prior to $0.01s$ shown in Figures 4 and 5. When corridors encompass physically unrealistic results, truncation of the corridors should be considered.

In each case, the proposed PCA/regression/Monte Carlo approach results in the corridor limits that not only have a narrower band but also can better reflect the shape of the original signal. The meaningful improvement associated with the current approach is that it produces corridors that are directly related to characteristics of the experimental data (e.g., the shoulder shape shown in Figure 5(b)). This is in contrast to traditional approaches for developing corridors, which average out aspects of curves related to subject anthropometry by applying the same normalization factor to an entire curve and then developing a corridor by taking the mean±SD of a set of responses normalized in this manner at each point in time.

Corridor limits constructed using the methods described in this chapter can be used for outlier detection by using a leave-one-out cross-validation technique where corridors are developed using all but one signal and the remaining signal is compared to the resulting corridor. Similarly, the method can be used to compare a subsequent response to a corridor developed from previous responses. However, further work is needed to set a reasonable criterion to evaluate signal's performance with respect to given corridor limits for the purposes of outlier detection.

A novel approach to generate response corridors for associated target body dimensions was developed. Unlike the traditional scaling and normalization approaches that assume relationships between response and anthropometry based on dimensional analysis or simple mechanical models-based relationships, the new method is based solely on statistical models derived from empirical data. An application of the new approach showed that it results in corridors that are narrower than traditional approaches to corridor development and captures curve shapes that are affected by body dimensions.

2.4 Acknowledgements

This work was funded under contract #N00024-13-D-6400, sponsored by the United States Army Research Lab in support of the Warrior Injury Assessment Manikin (WIAMan) project. Work at UMTRI was funded through subcontract #114322 from John Hopkins University Applied Physics Lab. The authors gratefully acknowledge input from Narayan Yoganandan from the Medical College of Wisconsin, Ian Marcus and Joel Stitzel from Wake Forest University, and Andrew Merkle and Liming Voo from the Johns Hopkins University Applied Physics Laboratory.

2.5 Conflict of interest statement

We wish to draw the attention of the Editor to the following facts which may be considered as potential conflicts of interest and to significant financial contributions to this work.

We confirm that the manuscript has been read and approved by all named authors and that there are no other persons who satisfied the criteria for authorship but are not listed. We further confirm that the order of authors listed in the manuscript has been approved by all of us.

We confirm that we have given due consideration to the protection of intellectual property associated with this work and that there are no impediments to publication, including the timing of publication, with respect to intellectual property. In so doing we confirm that we have followed the regulations of our institutions concerning intellectual property.

We understand that the Corresponding Author is the sole contact for the Editorial process (including Editorial Manager and direct communications with the office). He/she is responsible for communicating with the other authors about progress, submissions of revisions and final approval of proofs. We confirm that we have provided a current, correct email address which is accessible by the Corresponding Author and which has been configured to accept email from sunwbgtumich.edu

CHAPTER III

Confidence Band Development for Bivariate Functional Signal Responses using Gaussian Process Modeling

In this chapter, we discuss an approach to develop confidence bands for bivariate functional signal responses. The chapter is organized as follows: in Section 3.1, we will describe the notations, data structures and problem formulation. In Section 3.2, the Gaussian process model will be discussed in details, followed by the estimation technique. In Section 3.3, a case study for vehicle crash impact evaluation is demonstrated. The chapter then concludes with a summary.

3.1 Problem formulation

We begin with the description of the data structure using the crash test example described in Subsection 1.2.2. Let N denote the number of subjects that participate in the tests, each of which has p subject variables $X = \{x_i\}_{i=1,...,N} \in \mathbb{R}^{N\times p}$ including body measurements such as sitting height and BMI. For each subject i, a total of n_i replicate trials are conducted, generating profile signal responses at length L in two directions $d \in \{1, 2\}$. Let $\mathcal{T} = \{t_1, ..., t_L\}$ denote the time points where the signal responses are collected. The signal responses are represented by $\{y_{j,d}(x_i, t), t \in \mathcal{T}\}$ where j is the trial index and d is the direction index. Prior to applying the proposed method, the signals are assumed to be aligned in time. Curve registration approaches such as point-wise normalization (Gayzik et al., 2015) or moment method (James et al., 2007) are recommended to calculate the time delays.

There are three objectives to be achieved in the proposed method. Firstly, it is desired to generate predictive overall confidence bands of responses with any given subject variables x^* and time points t^*, which helps evaluate the vehicle safety for a specifically defined group of people who are not necessarily tested in the experiments. Let $y_d(x,t)$ denote the actual responses with any subject variables x, direction d and time point t where the subscript j is omitted for simplification. Constructing the overall confidence bands is equivalent to computing the predictive distribution of $y_d(x^*,t^*)$. Secondly, we would like to capture the functional profile shape by mapping signals of the first direction $y_1(x,t)$ and time t into those of the second direction $y_2(x,t)$. To compute the confidence bands, it requires to estimate the conditional distribution $y_2(x,t)|\{y_1(x,t), t\in\mathcal{T}\}$ for any $t\in\mathcal{T}$. In the end, it is of interests that abnormal trials needs to be detected. This result can help different facilities decide whether the trials for similar subjects can be combined to power the study. If the trial is detected to be abnormal, further investigation for the experimental conditions or subject settings is recommended. This can be accomplished by comparing the signal with the built confidence bands. For a given trial with subject variables x, an hypothesis test is established for this purpose:

$$\begin{aligned} H_0: &\quad \mathbb{E}\left[y_2(x,t)|\{y_1(x,t), t\in\mathcal{T}\}\right] = \mu_{2|1,t} \quad \text{for all } t\in\mathcal{T} \quad \text{versus} \\ H_1: &\quad \mathbb{E}\left[y_2(x,t)|\{y_1(x,t), t\in\mathcal{T}\}\right] \neq \mu_{2|1,t} \quad \text{for some } t\in\mathcal{T}, \end{aligned}$$

where $\mu_{2|1,t}$ is the conditional mean of the second direction given the magnitudes in the first direction for normal trials. The key issues to accomplish these objectives are to model $y_d(x,t)$, estimate the corresponding uncertainty and compute the conditional distribution. Detailed methodologies will be elaborated in the next section.

3.2 Methodology

3.2.1 Gaussian process modeling

In this subsection, the signal responses $y_{j,d}(x_i, t)$ is modelled in a non-parametric manner. To account for both the subject-to-subject variation and within-subject variation, the signal response $y_{j,d}(x_i, t)$ is decomposed into two independent terms as a mixed effect model as follows:

$$y_{j,d}(x_i, t) = f_d(x_i, t) + e_{i,j,d}(t), \tag{3.1}$$

where $f_d(x_i, t)$ denotes the mean response for subject variables x_i and $e_{i,j,d}(t)$ denotes the experimental errors among multiple replicate trials within each subject. As the subject variables only capture partial information of the human body, people with same subject variables may still have different responses in the test. Therefore the mean response $f_d(x_i, t)$ is a random function. The mean of the mean response is nonlinear with respect to both the time and subject variables to capture the subject effects since the subject variables' effects on the functional responses are often highly complicated and nonlinear. A non-parametric model is suggested to model the mean and variance of $f_d(x_i, t)$. Among all the non-parametric approaches, the Gaussian process modeling technique (Rasmussen and Williams, 2006) is selected for two reasons. First, building a confidence band that retains functional profile shape requires the conditional distribution of one direction given the other. It is convenient to compute the conditional distribution when the joint distribution of a Gaussian process is well-established. Second, the small sample size in the vehicle design applications makes some other non-parametric approaches not feasible. In the Gaussian process setting, the mean response $f_d(x, t)$ for any subject variable x is assumed to follow a Gaussian process with mean function $m(x, d, t)$ and covariance

function $c_f(d,t;d',t')$, which is written as

$$f_d(x,t) \sim \mathcal{GP}\left(m_d(x,t), c_f(d,t;d',t')\right), \tag{3.2}$$

where the subscript "f" represents function f. As a simplification, the within-subject error term $e_{i,j,d}(t)$ is assumed to be identically distributed among different subjects and repeated trials and hence is represented only with a random function of the direction d and time t only. We further assume the within-subject error term to follow a zero-mean Gaussian process as

$$e_{i,j,d}(t) \sim \mathcal{GP}\left(0, c_e(d,t;d',t')\right). \tag{3.3}$$

Substituting (3.2) and (3.3) into (3.1) yields the joint distribution of the functional responses as:

$$y_{j,d}(x_i,t) \sim \mathcal{GP}\left(m_d(x_i,t), c_f(d,t;d',t') + c_e(d,t;d',t')\right).$$

The conditional distribution is calculable once the joint distribution is well-defined, which requires modelling and estimating the mean function $m_d(x,t)$ and the two covariance functions $c_f(d,t;d',t')$ and $c_e(d,t;d',t')$.

3.2.2 Mean function

The true mean function is a nonlinear mapping from a joint space of subject variables, time points and different directions to the real space $\mathbb{R}$. To model the nonlinear relationship, we employ a two-step semi-parametric approach to link all the inputs with the mean responses. Firstly, the B-spline fitting technique is applied to decompose the mean responses into a series of basis functions $\{\phi_k(t)\}$ with the corresponding B-spline coefficients $\xi_{k,d}(x)$, that is,

$$m_d(x,t) = \sum_{k=1}^{K} \xi_{k,d}(x)\phi_k(t) + \varepsilon_1, \tag{3.4}$$

where the basis $\phi_k(t)$ is a pre-specified basis function while the coefficient $\xi_{k,d}(x)$ depends on subject variables x while ε_1 is the B-spline approximation error. After that, we employ a polynomial regression model for $\xi_{k,d}(x)$, which is to assume

$$\xi_{k,d}(x) = \sum_{l=1}^{p} \sum_{s=1}^{q} \beta_{k,l,d,s} x_{(l)}^{s} + \varepsilon_{2,k}, \tag{3.5}$$

where $x_{(l)}$ denotes the $l-$th direction of subject variables x and $\varepsilon_{2,k}$ denotes the regression error. Up to q-th order polynomial terms for each direction of subject variables x are used as the predictors, following an additive model setting without interaction terms between p subject variables. The polynomial regression model is selected because of its interpretability. Substituting (3.5) into (3.4) gives the approximated mean model as

$$m_d(x,t) = \sum_{k=1}^{K} \sum_{l=1}^{p} \sum_{s=1}^{q} \beta_{k,l,d,s} x_{(l)}^{q} \phi_k(t) + \varepsilon_1 + \sum_{k=1}^{K} \varepsilon_{2,k} \phi_k(t). \tag{3.6}$$

3.2.3 Covariance functions

After modeling the subject mean responses using nonparametric model in (3.6), the B-spline fitting and regression residuals need to be considered. Moreover, as subject variables are only subset of human body characteristics, people with same subject variables may still vary in other unobserved body characteristics, resulting in different functional responses. This source of variation is defined as subject randomness in this chapter. The subject randomness, B-spline approximation and regression errors contribute to the total between-subject uncertainties, which can be evaluated by $\psi_{f,d}(x_i,t) = \bar{y}_d(x_i,t) - \hat{m}_d(x_i,t)$, where

$$\bar{y}_d(x_i,t) = \frac{1}{n_i} \sum_{j=1}^{n_i} y_{j,d}(x_i,t)$$

represents the averaged responses and the estimated mean responses

$$\hat{m}_d(x,t) = \sum_{k=1}^{K} \sum_{l=1}^{p} \sum_{s=1}^{q} \hat{\beta}_{k,l,d,s} x_{(l)}^{q} \phi_k(t).$$

is obtained by substituting the estimated parameters $\hat{\beta}$ into (3.6). The within-subject errors are evaluated via $\psi_{e,d,j}(x_i,t) = y_{d,j}(x_i,t) - \bar{y}_d(x_i,t)$. A comparison between the between-subject uncertainties and the within-subject errors is shown in Figure 3.1 where $\{\psi_{f,d}(x_i,t), i = 1,...,N\}$ is compared with $\{\psi_{e,d,j}(x_i,t), i = 1,...,N, j = 1,...,n_1\}$. The two panels show the comparisons when $d = 1$. The differences in the variance scale and pattern motivate us to analyze the between-subject error and within-subject error separately using two Gaussian process models. The right panel of Figure 3.1 indicates that the within-subject error is identically distributed among all different subjects. The Gaussian process models are elaborated in the rest of this subsection.

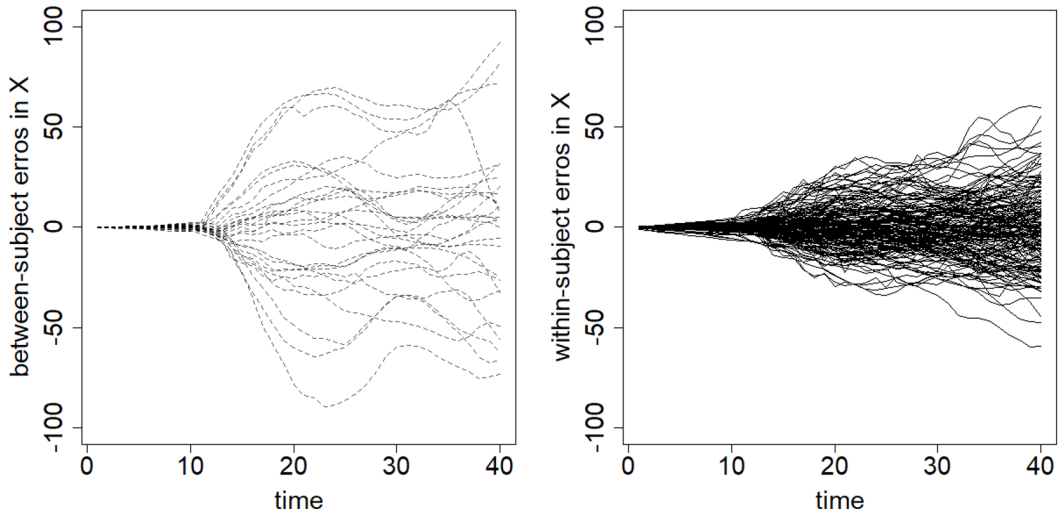

Figure 3.1: Comparison between different sources of variation.

It is commonly seen in the crash tests that the signal responses are non-stationary. In fact, the trajectory often shows an increasing trend at the beginning and then a decreasing trend after the force reaches the maximum. To consider these data characteristics, we decompose the covariance function $c_f(d,t;d',t')$ as the multiplication of the stationary cross-covariance term $c_{f,1}(d,d')$, the stationary auto-covariance term

$c_{f,2}(t,t')$ and non-stationary variances $v_{f,d}(t)$ and $v_{f,d'}(t')$. This decomposition relies on the widely-used separability assumption in the spatial-temporal literature (Gneiting et al., 2006) where the auto-covariance and cross-covariance are independent of each other. The decomposition is described as

$$c_f(d,t;d',t') = c_{f,1}(d,d') \times c_{f,2}(t,t') \times v_{f,d}(t) \times v_{f,d'}(t').$$

Then the cross-covariance term can further represented by a cross-correlation coefficient as:

$$c_{f,1}(d,d') = \sigma_{f,c}^{1-\delta(d,d')},$$

where $\delta(d,d')$ is the Kronecker's delta function that takes value of one when $d = d'$ and zero otherwise.

For the auto-covariance term, we select the Squared Exponential (SE) covariance structure to parametrize $c_{f,2}(t,t')$, which is written as

$$c_{f,2}(t,t') = \sigma_{f,d}^2 k_f(t,t') + \sigma_f^2 \delta(t,t'),$$
$$k_f(t,t') = exp\left\{-(t-t')^2/2l_f^2\right\},$$

where $\sigma_{f,d}^2$ is the variation magnitude, l_f is the length-scale and σ_f^2 is the nugget effect variance. Let $v_{f,d}(t)$ denote the variances of signal responses at time t and direction d. They are estimable since they are assumed to be identical among different subjects. In addition, the direction of Gram matrix is reduced to $2L \times 2L$ since the effect of subject variables x is removed. This simplification does not harm the convenience in generating confidence bands that capture functional profile shape since time t is still considered as an input of the covariance function. These parameters determine the Gaussian process and are required to be estimated prior to the prediction step.

The covariance function of within-subject errors is constructed similarly. In the first step, the covariance function $c_e(d,t;d',t')$ is decomposed into a station-

ary cross-covariance term $c_{e,1}(d, d')$, a stationary auto-covariance term $c_{e,2}(t, t')$ and non-stationary variances $v_{e,d}(t)$ and $v_{e,d'}(t')$, which is written as

$$c_e(d, t; d', t') = c_{e,1}(d, d') \times c_{e,2}(t, t') \times v_{e,d}(t) \times v_{e,d'}(t').$$

After that, the cross-covariance term is modeled based on the cross-correlation coefficients as:

$$c_{e,1}(d, d') = \sigma_{e,c}^{1-\delta(d,d')}.$$

The auto-covariance term is modeled under SE covariance structure as

$$c_{e,2}(t, t') = \sigma_{e,d}^2 k_e(t, t') + \sigma_e^2 \delta(t, t'),$$
$$k_e(t, t') = exp\left\{-(t - t')^2 / 2l_e^2\right\}.$$

As a summary, the covariance structure is illustrated in Figure 3.2. The Gaussian process model can be used for the prediction once all the parameters are estimated, which include $\beta_{k,l,d,s}$'s in the mean response, $v_{f,d}(t)$, $\sigma_{f,c}$, $\sigma_{f,d}$, σ_f and l_f in the subject-to-subject level covariance function, and $v_{e,d}(t)$, $\sigma_{e,c}$, $\sigma_{e,d}$, σ_e and l_e in the within-subject level covariance function. The next subsection will discuss the estimation techniques in details.

3.2.4 Parameters Estimation

As the number of regression parameters $\beta_{k,l,d,s}$ is $2Kpq$, we would like to divide the estimation procedure into two steps. First, the regression parameters in the mean model are estimated using regularized variable selection techniques. Then the parameters in the covariance functions are estimated via Maximum Likelihood (ML) approach.

Prior to estimating the regression parameters, the B-spline coefficients

$$\{\xi_{k,d}(x_i), k = 1, ..., K\}$$

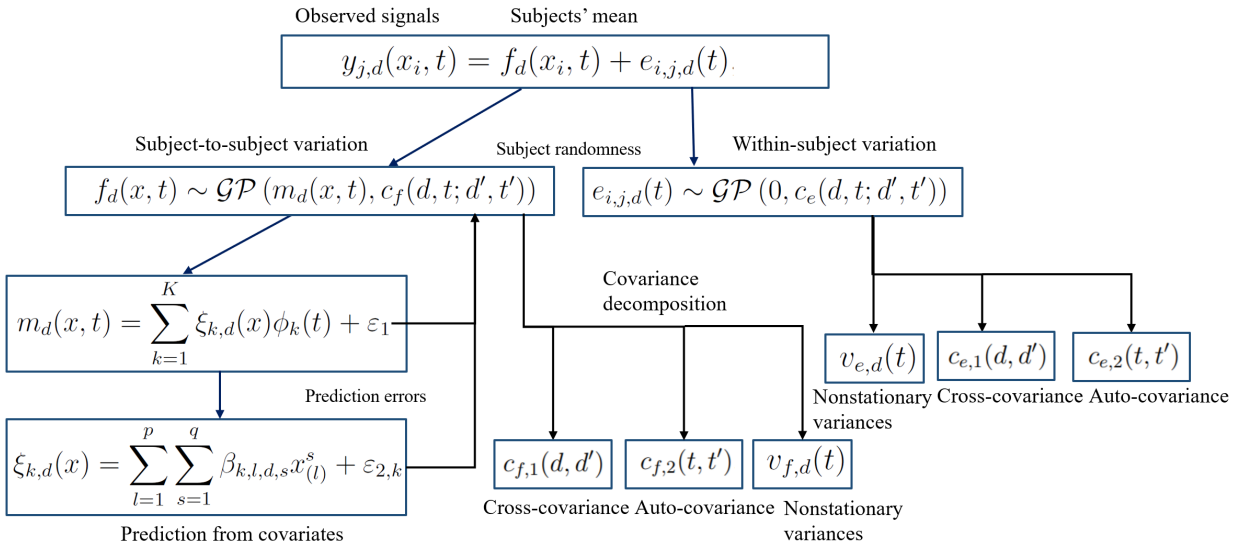

Figure 3.2: Detailed covariance structure.

are computed based on the averaged responses and the pre-specified B-spline basis. Let

$$\Phi = \begin{pmatrix} \phi_1(1) & ... & \phi_1(L) \\ ... & ... & ... \\ \phi_K(1) & ... & \phi_K(L) \end{pmatrix}$$

represent the matrix of B-spline basis, $\bar{\boldsymbol{y}}_d(x_i) = \{\bar{y}_d(x_i,1), ..., \bar{y}_d(x_i,L)\}$ represent the vectorized average responses. These estimators are

$$\hat{\boldsymbol{\xi}}_d(x_i) = (\Phi^T\Phi)^{-1}\Phi^T\bar{\boldsymbol{y}}_d(x_i),$$

where $\hat{\boldsymbol{\xi}}_d(x_i) = \left\{\hat{\xi}_{1,d}(x_i), ..., \hat{\xi}_{K,d}(x_i)\right\}$ is a collection of estimated B-spline coefficients for different basis. An estimate of the regression parameters

$$\hat{\beta}_{k,d} = \left\{\hat{\beta}_{k,1,d,1}, ..., \hat{\beta}_{k,1,d,q}, ..., \hat{\beta}_{k,p,d,1}, ..., \hat{\beta}_{k,p,d,q}\right\}$$

for given B-spline coefficient k and direction d are obtained from Lasso regression (Hastie et al., 2015) with polynomial predictors. Let

$$\mathsf{X} = \left\{\left(x_{(1)}^1\right)^T, ..., \left(x_{(1)}^q\right)^T, ..., \left(x_{(p)}^1\right)^T, ..., \left(x_{(p)}^q\right)^T\right\} \in \mathbb{R}^{n\times pq}$$

denote the matrix of polynomial predictors where $x_{(l)}^s$ denotes the $s-$th order of the $l-$th direction of subject variable x, the estimations are given as:

$$\hat{\beta}(k,d) = \arg\min_b \left\{ \left\| \hat{\boldsymbol{\xi}}(x_i,d) - \mathsf{X}b \right\|^2 + \lambda_{k,d} \sum_{k=1}^{p} |b| \right\}, \text{ for all } k = 1, ..., K; d = 1, 2,$$

where $\|\cdot\|$ represents the L_2 norm. The coefficient for the L_1 penalty term $\lambda_{k,d}$ is computed as the minimizer of the mean-squared errors in a 10-fold cross validation. First, we would like to use the fitting residuals $\psi_{f,d}(x_i,t) = \hat{m}_d(x_i,t) - \bar{y}_d(x_i,t)$ to estimate the non-stationary variances $v_{f,d}(t)$. The estimations are given as the sample variances of $\psi_{f,d}(x_i,t)$ as:

$$\hat{v}_{f,d}(t) = \frac{1}{N-1} \sum_{i=1}^{N} \psi_{f,d}^2(x_i,t).$$

Let $\theta_f = \{\sigma_{f,c}, \sigma_{f,d}, \sigma_f, l_f\}$ collect the rest of parameters of the subject-to-subject covariance function and $\psi_f(x_i) = \{\psi_{f,1}(x_i,t_1), ..., \psi_{f,1}(x_i,t_L), \psi_{f,2}(x_i,t_1), ..., \psi_{f,2}(x_i,t_L)\}$ collect the fitting residuals of all the time points and directions. Since the joint distribution of given points in a Gaussian process is still Gaussian with known mean and variance, the log-likelihood can be written as:

$$\begin{aligned} \log p\left(\psi_f(x_1), ..., \psi_f(x_N); \theta_f\right) = &-\frac{1}{2} \sum_{i=1}^{N} \psi_f^T(x_i) K_f^{-1}(\hat{v}_f, \theta_f) \psi_f(x_i) \\ &- \frac{1}{2} N \log |K_f(\hat{v}_f, \theta_f)| - \frac{NL}{2} \log 2\pi, \end{aligned}$$

where $K_f(\hat{v}_f, \theta_f)$ is the Gram matrix of c_f given all the parameters $\hat{v}_f$ and θ_f. The parameters θ_f are estimated via maximizing the log-likelihood, which is to compute

$$\hat{\theta}_f = \arg\max_\theta \log p\left(\psi_f(x_1), ..., \psi_f(x_N); \theta\right).$$

The parameters of the within-subject covariance function are estimated similarly. First, the within-subject residuals are calculated as

$$\psi_{e,d,j}(x_i,t) = y_{j,d}(x_i,t) - \bar{y}_d(x_i,t).$$

Their variances are used to estimate the non-stationary variances as

$$\hat{v}_{e,d}(t) = \frac{1}{\sum_{i=1}^{N} n_i - 1} \sum_{i=1}^{N} \sum_{j=1}^{n_i} \psi_{e,d,j}(x_i, t)^2.$$

Let $\theta_e = \{\sigma_{e,c}, \sigma_{e,d}, \sigma_e, l_e\}$,

$$\psi_{e,j}(x_i) = \{\psi_{e,1,j}(x_i, t_1), ..., \psi_{e,1,j}(x_i, t_L), \psi_{e,2,j}(x_i, t_1), ..., \psi_{e,2,j}(x_i, t_L)\}$$

and $\Psi = \{\psi_{e,j}(x_i); j \leq n_i, i \leq N\}$, the log-likelihood is expressed as

$$\log p\left(\Psi; \theta_e\right) = -\frac{1}{2} \sum_{i=1}^{N} \sum_{j=1}^{n_i} \psi_{e,j}^T(x_i) K_e^{-1}(\hat{v}_e, \theta_e) \psi_{e,j}(x_i) - \frac{N}{2} \log |K_e(\hat{v}_e, \theta_e)| - \frac{NL}{2} \log 2\pi,$$

where $K_e(\hat{v}_e, \theta_e)$ is the Gram matrix of c_e given all the parameters $\hat{v}_e$ and θ_e. Then maximizing the log-likelihood yields the estimates of θ_e as

$$\hat{\theta}_e = \arg\max_{\theta} \log p\left(\Psi; \theta\right).$$

3.2.5 Confidence bands construction and abnormal trials detection

After all the parameters are estimated, it is possible to generate the confidence bands. Before all the detailed derivations, a few additional definitions are introduced to simplify the notations. The observed responses are re-organized as a long vector in

$$\mathcal{Y}_j(x, \mathcal{T}) = \{y_{j,1}(x, t_i), y_{j,2}(x, t_i) : t_i \in \mathcal{T}, i = 1, ..., |\mathcal{T}|\}$$

and the unknown responses are re-organized as

$$\mathcal{Y}(x^*, \mathcal{T}) = \{y_1(x, t_i), y_2(x, t_i) : t_i \in \mathcal{T}, i = 1, ..., |\mathcal{T}|\}.$$

When considering both the subject-to-subject and within-subject variations, we combine the two terms as $c(d, t; d', t') = c_f(d, t; d', t') + c_e(d, t; d', t')$. To make the terms consistent, the mean responses are written as $m_d(x, \mathcal{T}) = \{m_d(x, t_i) : t_i \in \mathcal{T}, i = 1, 2, ..., |\mathcal{T}|\}$. Combining the two different directions yields the overall mean response

$m(x, \mathcal{T}) = \{m_1(x, \mathcal{T}), m_2(x, \mathcal{T})\}$. The covariance matrices are arranged in the similar way. Let

$$K_{d,d'}(\mathcal{T}, \mathcal{T}') = \{c(d, t_i; d', t_j) : t_i \in \mathcal{T}, i = 1, ..., |\mathcal{T}|, t_j \in \mathcal{T}', j = 1, ..., |\mathcal{T}'|\},$$

To evaluate the covariance functions at any unknown time point t^*, the estimated non-stationary variances $\hat{v}_{f,d}(t)$ and $\hat{v}_{e,d}(t)$ are extended to t^* based on B-spline basis $\{\phi_k(t), k = 1, ..., K\}$. The overall covariance matrix including both of the directions is expressed in

$$K(\mathcal{T}, \mathcal{T}') = \begin{pmatrix} K_{1,1}(\mathcal{T}, \mathcal{T}') & K_{1,2}(\mathcal{T}, \mathcal{T}') \\ K_{2,1}(\mathcal{T}, \mathcal{T}') & K_{2,2}(\mathcal{T}, \mathcal{T}') \end{pmatrix}_{2|\mathcal{T}| \times 2|\mathcal{T}'|}.$$

These notations will help establish the derivations in the following paragraphs.

To begin with, we would like to generate an overall confidence band for the responses $y_d(x, t)$ for given subject variables x^* and a set of time points $\mathcal{T}^* = \{t_1^*, ...t_{L^*}^*\}$. Since the covariances only depend on time and direction, we write the joint distribution of $\mathcal{Y}_j(x, \mathcal{T})$ and $\mathcal{Y}(x^*, \mathcal{T}^*)$ as

$$\begin{pmatrix} \mathcal{Y}_j(x, \mathcal{T}) \\ \mathcal{Y}(x^*, \mathcal{T}^*) \end{pmatrix} \sim \mathcal{N}\left(\begin{pmatrix} m(x, \mathcal{T}) \\ m(x^*, \mathcal{T}^*) \end{pmatrix}, \begin{pmatrix} K(\mathcal{T}, \mathcal{T}) & K(\mathcal{T}, \mathcal{T}^*) \\ K(\mathcal{T}^*, \mathcal{T}) & K(\mathcal{T}^*, \mathcal{T}^*) \end{pmatrix} \right), \tag{3.7}$$

Therefore, the predictive distribution of $\mathcal{Y}(x^*, \mathcal{T}^*)$ is a Gaussian distribution with mean $m_c(x^*, \mathcal{T}^*)$ and covariance K_c shown as follows:

$$m_c(x^*, \mathcal{T}^*) = m(x^*, \mathcal{T}^*) + K(\mathcal{T}^*, \mathcal{T}) K^{-1}(\mathcal{T}, \mathcal{T}) \left(\mathcal{Y}_j(x, \mathcal{T}) - m(x, \mathcal{T})\right),$$

$$K_c = K(\mathcal{T}^*, \mathcal{T}^*) - K(\mathcal{T}^*, \mathcal{T}) K^{-1}(\mathcal{T}, \mathcal{T}) K(\mathcal{T}, \mathcal{T}^*).$$

They are calculable by substituting the unknown true parameters with the estimated parameters shown in Subsection 3.2.4. Combining the predictive distributions pointwisely produces a visualization of the confidence bands. The bands are consist of a series of ellipses generated from $\mathcal{N}\left(m_c(x^*, t), K_c(t, t)\right)$ for all the time points $t \in \mathcal{T}^*$.

Besides the predictive distribution for both of the two directions, it is of the researcher's interest to build the confidence bands that capture the functional profile shape. As was discussed in Section 3.1, we aim to compute the conditional distribution $y_2(x^*, \mathcal{T}^*)\big|\{y_1(x^*, \mathcal{T}^*)\}$ where $\boldsymbol{y}_d(x, \mathcal{T}) = \{y_d(x, t_i) : t_i \in \mathcal{T}, i = 1, ..., |\mathcal{T}|\}$. The joint distribution of the two is written as

$$\begin{pmatrix} y_1(x^*, \mathcal{T}^*) \\ y_2(x^*, \mathcal{T}^*) \end{pmatrix} \sim \mathcal{N}\left(\begin{pmatrix} m_1(x, \mathcal{T}^*) \\ m_2(x, \mathcal{T}^*) \end{pmatrix}, \begin{pmatrix} K_{1,1}(\mathcal{T}^*, \mathcal{T}^*) & K_{1,2}(\mathcal{T}^*, \mathcal{T}^*) \\ K_{2,1}(\mathcal{T}^*, \mathcal{T}^*) & K_{2,2}(\mathcal{T}^*, \mathcal{T}^*) \end{pmatrix} \right).$$

Hence the conditional distribution is Gaussian with mean $m_{c,2|1}(x^*, \mathcal{T}^*)$ and covariance $K_{c,2|1}$ computed as

$$\begin{aligned} m_{c,2|1}(x^*, \mathcal{T}^*) &= m(x, 2, \mathcal{T}^*) + K_{2,1}(\mathcal{T}^*, \mathcal{T}^*) K_{1,1}^{-1}(\mathcal{T}^*, \mathcal{T}^*) \left(\boldsymbol{y}_1(x, \mathcal{T}) - m_1(x, \mathcal{T}^*)\right), \\ K_{c,2|1} &= K_{2,2}(\mathcal{T}^*, \mathcal{T}^*) - K_{2,1}(\mathcal{T}^*, \mathcal{T}^*) K_{1,1}^{-1}(\mathcal{T}^*, \mathcal{T}^*) K_{1,2}(\mathcal{T}^*, \mathcal{T}^*). \end{aligned} \tag{3.8}$$

The conditional distribution in (3.8) gives two byproducts. First, it can be used to generate confidence bands point-wisely by combining $\mathcal{N}\left(m_{c,2|1}(x^*, t), Kc, 2|1(t, t)\right)$ for all the time points $t \in \mathcal{T}^*$. It gives a direct visualization of the confidence bands but may neglect the auto-covariance between time points.

The other byproduct is a systematic way for testing and removing abnormal trials without neglecting any auto-covariance. For the hypothesis testing:

$$\begin{aligned} H_0 : &\quad \mathbb{E}\left[y_2(x, t)|\{y_1(x, t), t \in \mathcal{T}\}\right] = \mu_{2|1,t} \quad \text{for all } t \in \mathcal{T} \quad \text{versus} \\ H_1 : &\quad \mathbb{E}\left[y_2(x, t)|\{y_1(x, t), t \in \mathcal{T}\}\right] \neq \mu_{2|1,t} \quad \text{for some } t \in \mathcal{T}, \end{aligned}$$

the test statistic C is calculated for comparing the actual second direction of the signal $\boldsymbol{y}_2(x^*, \mathcal{T}^*)$ with the conditional distribution shown in (3.8). It is

$$C = \left(\boldsymbol{y}_2(x^*, \mathcal{T}^*) - \hat{m}_{c,2|1}(x^*, \mathcal{T}^*)\right)^T \hat{K}_{c,2|1}^{-1} \left(\boldsymbol{y}_2(x^*, \mathcal{T}^*) - \hat{m}_{c,2|1}(x^*, \mathcal{T}^*)\right).$$

where $\hat{m}_{c,2|1}$ and $\hat{K}_{c,2|1}$ are calculated by substituting the estimated parameters into the true parameters. Therefore C is asymptotically χ^2 distributed with L degrees

of freedom. A trial is considered to be abnormal if $C > \chi^2_{L,1-\alpha}$ where α is the pre-specified significance level. For any detected trial, further investigation for the experimental conditions or subject settings is recommended.

3.3 Results

In this section, we present an analysis of data in the vehicle design application. 28 children and 2 adults are involved in the crash tests to validate the seat designs at the Children's Hospital of Philadelphia. The 30 subjects have various body features (subject variables). Among all the subject variables, 4 important ones are selected as the predictors based on the domain knowledge, which are age, sitting heights, body mass and iliac crest heights. To address the non-linearity, we further expand the 4 directional predictor set to $p = 16$ by including up to $4-$th order of polynomial terms. For each subject, up to 6 identical trials are conducted to capture the measurement errors. During each trial, the sensor installed on the geometric center of the head recorded the three-directional trajectories. A total of $L = 40$ trajectory points are uniformly sampled with $10Hz$ frequency. The trajectories along the lateral direction are considered less important and hence removed. For the convenience in demonstration, we label the vertical direction as Z axis and $d = 2$ while the horizontal direction as X axis and $d = 1$. Prior to applying the proposed method, the trajectories are aligned by maximizing the cross-covariance between the trajectories in the vertical direction.

The confidence bands are then constructed according to the proposed method. The $5-$th subjects' responses are selected to demonstrate the method. The head trajectories recorded during the 6 identical trials are shown in the top panel of Figure 3.3 where the within-subject point-wise variations of $y_{j,2}(x_5, t)$ is larger than

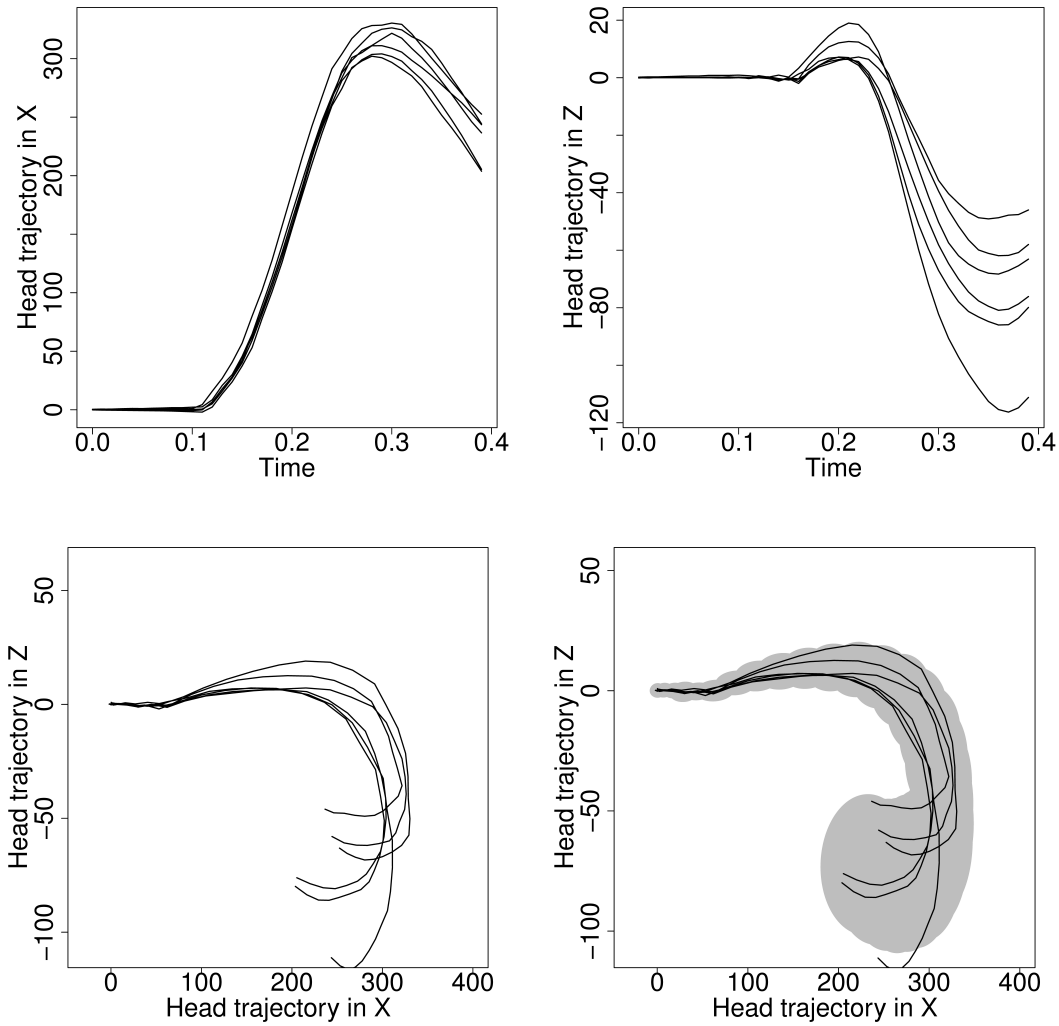

Figure 3.3: Overall confidence band for a selected subject. Top left panel: head trajectories along X direction; top right panel: head trajectories along Z direction; bottom left panel: bivariate head trajectories showing the functional profile shape; bottom right panel: generated overall confidence band via the proposed method.

$y_{j,1}(x_5, t)$. The right panel also shows an increasing trend of point-wise variances with time, implying the non-stationary issue. Plotting $y_{j,1}(x_5, t)$ versus $y_{j,2}(x_5, t)$ generates the bivariate head trajectories during the crash tests, which is shown in the bottom left panel of Figure 3.3. They share a similar pattern that the head geometric center will be pushed forward and then be pulled backward and downward after it reaches the furthest point. The functional profile shape makes it impossible to model $y_{j,2}(x_5, t)$ as a function of $y_{j,1}(x_5, t)$ directly. The bottom right panel of Figure 3.3 depicts the overall two-standard-deviation confidence band in (3.7). The confidence band is generated with a time frequency of $100Hz$ to guarantee its smoothness. The band has a high coverage rate on the signal responses and retains the similar functional profile shape as the signal responses.

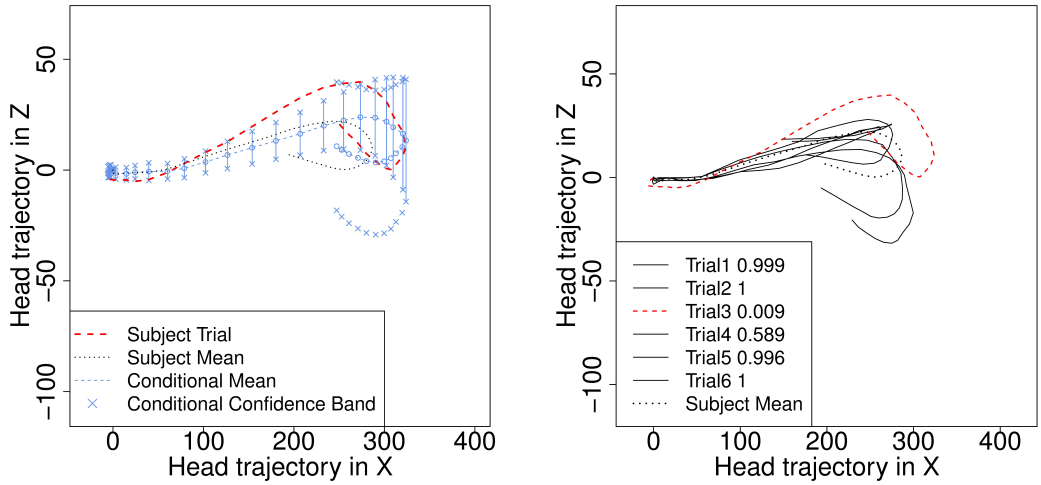

Figure 3.4: Conditional confidence band and hypothesis testing results for a selected subject. Left panel: the confidence band of $y_{3,2}(x_4, t)$ given $y_{3,1}(x_4, t)$; right panel: the p-values of hypothesis testings, the third trial is detected as an outlier as its p-value is smaller than 0.05.

Then we select the $4-$th subject to demonstrate the conditional confidence band and abnormal trial detection method where the third trial appears to be different from the others. The conditional confidence band of $\{y_{3,2}(x_4, t), t \in \mathcal{T}\}$ given

$\{y_{3,1}(x_4, t), t \in \mathcal{T}\}$ is constructed via (3.8) and shown in the left panel of Figure 3.4 where the coverage rate for the actual response signal is small. To locate the abnormal signals, the proposed hypothesis testing is ran for all the trials' responses, generating p-values in the right panel of Figure 3.4. The p-value of the third trial is $0.009 < \alpha = 0.05$, suggesting the removal of this trial from the set of subject responses.

3.4 Summary

In this chapter, we present a new method to construct confidence bands for bivariate functional signals. The effect of subject variables is quantified by non-parametric B-spline fitting technique and a polynomial regression model, which is capable for non-linear dependencies between the subject variables and functional signals. The complicated covariance structure is captured by a Gaussian process. It is decomposed into within-subject variability, auto-covariance between time points and cross-covariance between different directions, which can be further used for generating confidence bands to capture the bivariate functional profile shape. The developed model is effectively used for testing abnormal functional responses based on the property of Gaussian process. For the Gaussian process model, a two-stage estimation procedure is used to obtain the estimates of parameters. This may not accurately estimate the uncertainty as the parameters are assumed known before moving onto estimating another set of parameters. A full Bayesian framework is recommended to solve this estimation issue in the future work to construct more realistic confidence bands.

CHAPTER IV

Robust System Design Optimization with Limited Experimental Data and An Inexact Simulation Model

In this chapter, we propose a method for design optimization that considers both sources of uncertainty from parameters and model inexactness. For solving the research challenges discussed in Subsection 1.2.3, the proposed method involves two steps: (1) computing feasible regions for the computer simulation parameters and model bias; and (2) searching for optimal design solutions under a robust optimization formulation. In Section 4.1, we will describe the notations, data structures and formulate the problem. In Section 4.2 and Section 4.3, the proposed method is described to account for parameter uncertainty and model inexactness with a robust optimization formulation. In Section 4.4, model assumptions and statistical properties are elaborated in three theorems. In Section 4.5, a numerical illustration is provided for methodology illustration, followed by a case study for vehicle restraint components design optimization in Section 4.6. The chapter then concludes with a discussion.

4.1 Notation, data structure and objective

Our setting will have $\mathcal{X}$ denote the space of q design variables of interest. For each $x \in \mathcal{X}$, say that there is a corresponding length L response which represents the system response. In our example of vehicle crash test, this is a time series of the measured head acceleration as the crash occurs. The performance evaluation

function $J : \mathbb{R}^L \to \mathbb{R}$ converts the time series response into a single value to be optimized. For simplicity, the evaluation function is negatively oriented (smaller is better). In our example, J is closely related to the maximum of the head acceleration within the time series. Then, the optimal design is defined in the following sense. Let $\zeta : \mathcal{X} \to \mathbb{R}^L$ represent the true response from the system, the optimal design can be chosen as

$$x^* = \arg\min_{x \in \mathcal{X}} J\left(\zeta(x)\right).$$

However, because crash tests are expensive, only sparse design configurations are tested. We do not know the true system response at all x, so this optimization problem cannot be solved but represents the oracle's benchmark.

The simulation model maps an input and a parameter to a time series. The simulation model is denoted by $\eta : \mathcal{X} \times \Theta \to \mathbb{R}^L$. Ideally, $\eta(x, \theta)$ represents the expected result if we were to conduct a physical experiment at x if the parameter is θ. In reality, $\eta(x, \theta)$ may not be exactly equal to $\zeta(x)$ for all x. This implies that if $\eta(x, \theta)$ is used to search for x^*, the resultant optimal design may not be equal to

$$\arg\min_{x \in \mathcal{X}} J\left(\eta(x, \theta)\right).$$

Thus we aim to choose a good estimate of x^* using our collected experimental data. Assume n physical tests are conducted in the design space at $X = \{x_i\}_{i=1,\ldots,n}$, which is a subset of $\mathcal{X}$. For each of these tests, there is a vector $y_i = (y_{i1}, ..., y_{iL})$ which collects the response measurements with a length L from the real system. In our example of vehicle crash tests, y_i is a time series of head acceleration measurements observations as a crash occurs.

The choice of design can be multifaceted, thus we will produce three separate data products. Firstly, we would like to estimate x^* with some value $\hat{x}$ based on

our testing data. In terms of statistical objectives, we would like consistency in terms of our objective. That is, as n gets large, we would like $\hat{x}$ to converge to x^*. Secondly, we would like to place a upper confidence bound on the performance of the chosen design by finding some $\widehat{J}(x)$ such that $\widehat{J}(x) > J(\zeta(x))$ with some minimum confidence level $1-\alpha$. The upper confidence bound is used to evaluate the worst-cases in the robust optimal design. Lastly, we would like to produce a confidence set for the design variables $\widehat{\mathsf{X}}$. We would like $\widehat{\mathsf{X}}$ to include x^* with at least a prescribed probability $1-\alpha$ as n gets large.

We consider three types of uncertainties when optimizing the design:

(a) *Observation error:*

Observation error, denoted by ε_i, a length L vector, is the difference between the physical test responses y_i and the underlying true physical system responses $\zeta(x_i)$, thus

$$y_i = \zeta(x_i) + \varepsilon_i.$$

For simplicity, we presume ε_i is a vector of independent and identically distributed normal random variable with a zero mean and a known variance σ^2. The value of σ^2 is assumed to be known, but it could also be estimated separately with some minor changes to the proposed method.

(b) *Model bias:*

Simulation models are used for predicting the true physical system response but not always exact. Thus, a computer model needs to be corrected with an unknown model bias term denoted by δ, which maps the design variable and a parameter to $\mathbb{R}^L$ and is defined by

$$\delta(x,\theta) = \zeta(x) - \eta(x,\theta) \tag{4.1}$$

this term is also known as model inadequacy.

(c) *Parameter uncertainty:*

The computer simulation parameters are required to generate system simulation responses. These parameters have unignorable impacts on the system responses. Simulation parameters can represent the physical constants whose true values are fixed but not observable in the physical tests. In the crash tests, the seat friction depends on the cloth material, experiment temperature, initial sitting position and some other factors. We do not distinguish between these cases in our approach as we leave the true parameters undefined in our setting. As will be shown, robustness approaches do not require a definition of the parameters.

4.2 Overview of the approach

The objective of this study is to search for an optimal robust design with respect to the system performance evaluation function in light of these three sources of uncertainty. We can rewrite the ideal optimization problem as

$$x^* = \arg\min_{x \in \mathcal{X}} J(\eta(x, \theta) + \delta(x, \theta)).$$

If η is known, or at least computable, the key issue of estimating x^* is to estimate θ and $\delta(x, \theta)$. Say that $\hat{\theta}$ is an estimate of θ while $\hat{\delta}(x, \theta)$ is an estimate of $\delta(x, \theta)$ given the physical tests responses, the non-robust estimate of the optimal design is chosen by

$$\hat{x}^{\mathrm{NR}} = \arg\min_{x \in \mathcal{X}} J(\eta(x, \hat{\theta}) + \hat{\delta}(x, \hat{\theta})).$$

In this way, the estimators $\hat{\theta}$ and $\hat{\delta}(x, \theta)$ does not incorporate any robustness principles. Instead of estimating θ and $\delta(x, \theta)$, say we are able to bound both θ and $\delta(x, \theta)$ in some region Θ and $\Delta(x, \theta)$ with some probabilistic guarantees, respectively and

then apply the minimax robust optimization technique (Verdu et al., 1984) to search for the optimal design. This involves two steps: in the "max" step, the worst-cases considering both the parameter uncertainty and the model bias are evaluated as the $1-\alpha$ upper confidence bounds of the true injury value $J(\zeta(x))$ according to the definition

$$\widehat{J}(x) = \max_{\theta\in\Theta} \max_{d\in\Delta(x,\theta)} J(\eta(x,\theta)+d). \tag{4.2}$$

In the "min" step, the robust design $\hat{x}^R$ minimizes the worst-cases, which is formulated as

$$\hat{x}^{\mathrm{R}} = \arg\min_{x\in\mathcal{X}} \widehat{J}(x). \tag{4.3}$$

Lastly, in contrast to the point estimation given in (4.3), an alternative interval estimation of x^* is proposed in (4.4) as

$$\widehat{\mathsf{X}} = \left\{ \xi \in \mathcal{X} \,\middle|\, \min_{\theta\in\Theta} \min_{d\in\Delta(\xi,\theta)} J\left(\eta(\xi,\theta)+d\right) \le \min_{x\in\mathcal{X}} \max_{\theta\in\Theta} \max_{d\in\Delta(x,\theta)} J(\eta(x,\theta)+d) \right\}. \tag{4.4}$$

We would like this set $\widehat{\mathsf{X}}$ to contain potentially optimal settings of the design variables. Both the point and interval estimates become well defined once we define $\Delta(x,\theta)$ and Θ based on the data. The next section will discuss the construction of these two objects given in (4.3) and (4.4) in details.

4.3 Finding $\Delta(x,\theta)$ and Θ based on data

In this section, the detailed methodology for finding $\Delta(x,\theta)$ and Θ is elaborated. Discovering $\Delta(x,\theta)$ based on data represents the major challenges. The objective of adding a bias term to the computer simulation model is to improve the fitting performance for the physical responses. Therefore we aim to define the feasible bias set $\Delta(x,\theta)$ as the constraint on the distance between the actual physical response and the computer simulation response when the bias is included. As the actual

physical response and the computer simulation response can be time series, the bias also takes the time series form. The feasible region of bias is established based on the $L2$ norm of the time series as

$$\{d : \|\eta(x,\theta) + d - \zeta(x)\| \leq \tau_e(x,\theta)\},$$

where the subscript e denotes fitting errors, $\tau_e(x,\theta)$ is the tolerance on the fitting error and $\|\cdot\|$ denotes the $L2$ norm of time series responses. Here we allow $\tau_e(x,\theta)$ to be a function of design points and simulation parameters' values to enhance the model flexibility. $L2$ norm is selected to guarantee the convexity of the feasible region of bias in the optimization step. It can be replaced by any other norm that guarantees the convexity. Substituting (4.1) into the above constraint simplifies it as a constraint on the distance between the feasible biases and the true bias, which is

$$\{d : \|d - \delta(x,\theta)\| \leq \tau_e(x,\theta)\}.$$

The above feasible set is not achievable because the true bias $\delta(x,\theta)$ is not known. We apply the nonparametric kernel regression technique to give an estimate as

$$\tilde{\delta}_n(x,\theta) = \frac{\sum_{i=1}^{n} K(H^{-1}(x_i - x))\delta_i(\theta)}{\sum_{i=1}^{n} K(H^{-1}(x_i - x))},$$

where K is the multivariate Kernel function $K(u) = \prod_{i=1}^{q} k(u_i)$ given any univariate Kernel function $k(\cdot)$. H is the diagonal bandwidth matrix with elements $\{h_1, ..., h_q\}$. $\delta_i(\theta) = y_i - \eta(x_i,\theta)$. Note that $delta_i(\theta)$ and $\tilde{\delta}_n(x,\theta)$ are vectors of length L when the responses are time series of length L. The univariate Kernel function $k : \mathbb{R} \to \mathbb{R}$ is required to satisfy the following assumption to guarantee the properties of kernel regression:

Assumption 1 $k(x) = k(-x)$, $\int_{-\infty}^{\infty} k(x)dx = 1$ and $k(0)$ is the maximum of $k(\cdot)$ in $\mathbb{R}$.

This assumption is typically seen in the definitions of Kernel functions. Further assumptions are imposed to the multivariate Kernel function K to guarantee consistency, which are

Assumption 2 $|K(u)| \leq \bar{K} < \infty$ and $\int_{\mathbb{R}^q} |K(u)|du \leq \bar{U} < \infty$.

Assumption 3 For some $\Lambda_1 < \infty$ and $U < \infty$, either $K(u) = 0$ for $\|u\| > U$ and for all $u, u' \in \mathbb{R}^q$, $\|K(u) - K(u')\| \leq \Lambda_1 \|u - u'\|$,

or $K(u)$ is differentiable, $|(\partial/\partial u)K(u)| \leq \Lambda_1$, and for some $\nu > 1$, $|(\partial/\partial u)K(u)| \leq \Lambda_1 \|u\|^{-\nu}$ for $\|\nu\| > U$.

Assumption 4 $h_j = Cn^{-1/(q+4)}$.

Assumptions 2 assumes that the kernel function $K(u)$ is bounded and integrable. Assumption 3 requires $K(u)$ to be smooth. The kernel function should either have truncated support and be Lipschitz or have a bounded derivative with an integrable tail. The two assumptions 2 and 3 allow for most kernels. Assumption 4 specifies bandwidth to guarantee the convergence rate. Assumptions 1-4 are part of the sufficient conditions for the uniform consistency shown in Hansen (2008).

To capture the randomness generated by the observation error, the tolerance on the fitting error $\tau_e(x, \theta)$ is calculated according to the asymptotic variance of the Kernel regression (Nadaraya, 1964; Watson, 1964) as

$$\tau_e(x, \theta) = \sqrt{\chi^2_{L,1-\alpha} \frac{R(k)^q \sigma^2}{nh_1 ... h_q \hat{f}(x)}},$$

where α is the significance level, $R(k) = \int k(u)^2 du$ and $\hat{f}(x) = \frac{1}{n|H|} \sum_{i=1}^{n} K(H^{-1}(x_i - x))$. When the variance of observation errors σ^2 is known, τ_e is determined by $\hat{f}(x)$ and therefore only depends on design variables. When σ^2 is not given, a consistent estimator

$$\hat{\sigma}^2(\theta) = \frac{1}{nL - 1} \sum_{i=1}^{n} \left\| y_i - \eta(x_i, \theta) - \tilde{\delta}_n(x_i, \theta) \right\|^2,$$

is used to approximate σ^2. The consistency is guaranteed by the following two assumptions where the observation errors are assumed to be independent and identically distributed among different observations and time points.

Assumption 5 $\{x_i\}_{i=1,...,n}$ are independently sampled.

Assumption 6 $\varepsilon_i \sim N(0, \sigma^2 I_L)$, where I_L is the identical matrix with dimension $L \times L$.

In this manner, $\tau_e(x, \theta)$ is a function of design points and simulation parameters' values. With an estimate of $\delta(x, \theta)$ and a well-defined tolerance value $\tau_e(x, \theta)$, the feasible set of the model bias is formally defined as

$$\Delta(x, \theta) = \left\{ d : \left\| d - \tilde{\delta}_n(x, \theta) \right\| \leq \tau_e(x, \theta) \right\}.$$

Besides the major challenges of discovering $\Delta(x, \theta)$, an explicit definition of Θ is required in practice to reduce the estimator variance when the sample size is small, which also reduces the computational load for generating simulation outputs in $\mathcal{X} \times \Theta$. Now we are going to specify a constraint and eliminate infeasible simulation parameters. For this purpose, a constraint on the differences between the experiment responses and the corresponding simulation outputs is imposed, which defines the feasible set of simulation parameters as

$$\Theta = \{\theta : \|y_i - \eta(x_i, \theta)\| \leq \tau_b, \text{ for any } i \in \{1, ..., n\}\}, \tag{4.5}$$

where τ_b is the threshold to be specified based on the domain knowledge of the simulation accuracy. This constraint guarantees that the simulation responses without adding bias term can predict the physical system at a certain level in all the experimental settings, which can be used to select the feasible simulation parameters.

$\Delta(x, \theta)$ is established for feasible bias of dimension L. Evaluating the worst-cases in (4.2) requires high computational resources for long time series responses of

length L. In practice, nonparametric basis approximation is recommended to reduce the dimension of functional responses. Let $M \in \mathbb{R}^{L\times S}$ denote the matrix of any basis functions where S is the number of basis. The time series responses can be approximated by $M\beta$ where β represents the corresponding coefficients. The feasible region of bias is converted into that of coefficients, which is

$$\mathcal{B}(x,\theta) = \left\{ b : \left\| Mb - \tilde{\delta}_n(x,\theta) \right\| \leq \tau_e(x,\theta) \right\}.$$

The worst-case evaluation equation in (4.2) and the interval estimator in (4.4) are revised accordingly as:

$$\widehat{J}(x) = \max_{\theta\in\Theta} \max_{b\in\mathcal{B}(x,\theta)} J(\eta(x,\theta) + Mb),$$

and

$$\widehat{\mathsf{X}} = \left\{ \xi \in \mathcal{X} \left| \min_{\theta\in\Theta} \min_{b\in\mathcal{B}(\xi,\theta)} J\left(\eta(\xi,\theta) + Mb\right) \leq \min_{x\in\mathcal{X}} \max_{\theta\in\Theta} \max_{b\in\mathcal{B}(x,\theta)} J(\eta(x,\theta) + Mb) \right. \right\}.$$

4.4 Statistical properties of the approach

The point estimator $\hat{x}^R$ and the confidence set $\widehat{\mathsf{X}}$ are calculable once $\Delta(x,\theta)$ and Θ are well defined. Now we are going to show the three statistical properties. In what follows, we will make the following additional assumption to develop the first theorem.

Assumption 7 For some $\Lambda_2 < \infty$ and for all $y, y' \in \mathbb{R}^L$, $\|J(y) - J(y')\| \leq \Lambda_2 \|y - y'\|$.

Assumptions 1-5 are the sufficient conditions for the uniform consistency of $\tilde{\delta}_n(x,\theta)$ according to Hansen (2008). Assumption 5 requires independent sampling, which is stronger than the $\alpha-$mixing assumption in Hansen (2008). Assumption 6 requires independence not only among different experiments but also among different time points. This extends the uniform consistency of univariate responses to that of

functional responses. Assumption 7 is a sufficient condition to transit the uniform consistency of the estimated bias into that of the estimated injury function which is shown in the following theorem.

Theorem 1: Suppose Assumptions 1-7 hold, then

$$\sup_{x\in\mathcal{X}}\left|\widehat{J}(x)-J(\zeta(x))\right|\to 0 \text{ as } n\to\infty.$$

Theorem 1 shows the uniform convergence property of the evaluation function. That is, when the sample size of physical experiments n goes large, the evaluation function $\widehat{J}(x)$ will approximate the true evaluation function $J(\zeta(x))$. The sample size n to achieve the given approximation accuracy will be independent of the selection of $x\in\mathcal{X}$. The convergence rate of the evaluation function is not given although the uniform convergence rate of $\tilde{\delta}_n(x,\theta)$ can be derived as an extension of Hansen (2008). This requires stronger assumptions on the injury function J and its derivatives. However, in some engineering applications, these assumptions may not hold. A counter example can be achieved by setting $J(y)=\max\{y_l,\, l\in\{1,...,L\}\}$, which is used to evaluate the thorax injury via maximal thorax deflection. In this case, the injury function is not differentiable. To ensure the consistency of the robust optimal deisgn $\hat{x}^R$, additional assumptions are added as follows:

Assumption 8 $\inf_{\|x-x^*\|>\varepsilon} J(\zeta(x))\geq J(\zeta(x^*))+\tau$, for some $\tau>0$.

Assumption 9 $\widehat{J}(\hat{x}^R)\geq\widehat{J}(x^*)-o_p(1)$.

Assumptions 8-9 resemble the assumptions for the consistency of M-estimator (Huber, 2011). Assumption 8 is the weaker version of the identification property assuming that x^* is the unique minimizer of the evaluation function $J(\zeta(\cdot))$. Assumption 9 ensure that the distance between the minimum of $\widehat{J}(\cdot)$ and $\widehat{J}(x^*)$ are smaller than $o_p(1)$, which can be used to derive the upper bound of $J(\zeta(\hat{x}^R))-J(\zeta(x^*))$. Com-

bining this result with the uniform consistency of the estimated evaluation function $\widehat{J}(\cdot)$ yields the consistency of the proposed robust estimator. The results is shown in the following corollary.

Corollary 1: Suppose Assumptions 1-9 hold, $\hat{x}^R \to_p x^*$ as $n \to \infty$.

This result is intuitive because the optimal design can be directly identified from the experiment data when an extremely large number of physical experiments are conducted. In this way, the selection of simulation parameters or even the computer simulation responses is not important in determining the optimal design. The asymptotic distribution of $\tilde{\delta}_n(x, \theta)$ can be derived based on Assumption 10, which is:

Assumption 10 $\delta(x, \theta)$ is second-order differentiable with respect to x.

With the asymptotic distribution, an $1 - \alpha$ upper confidence bound of the actual evaluation function $J(\zeta(x))$ can be computed according to the following theorem.

Theorem 2: Under Assumptions 1-7 and Assumption 10, for all $x \in \mathcal{X}$,

$$\mathbb{P}\left[\widehat{J}(x) \geq J(\zeta(x))\right] \geq 1 - \alpha \text{ as } n \to \infty.$$

The upper confidence bound is used to evaluate the worst-cases and formulate the minimax robust optimization. Intuitively, the worst-cases should be evaluated within a reasonable range considering the observation error. This theorem provides a theoretical way to calculate the injury values of the worst-cases according to the asymptotic distribution of the Kernel regression estimator $\tilde{\delta}_n(x, \theta)$.

Theorem 3: Suppose Assumptions 1-7 hold, $\mathbb{P}\left[x^* \in \widehat{\mathsf{X}}\right] \geq 1 - \alpha$ as $n \to \infty$.

Theorem 3 assures the coverage rate of the proposed interval estimates, which guarantees the probability that the true optimal design falls within the confidence set is greater than $1-\alpha$ when the sample size n goes large. This is a loose confidence

set with asymptotic coverage probability of one since

$$\min_{\theta\in\Theta}\min_{d\in\Delta(x^*,\theta)} J\left(\eta(x^*,\theta)+d\right) \leq \max_{\theta\in\Theta}\max_{d\in\Delta(\hat{x}^R,\theta)} J(\eta(\hat{x}^R,\theta)+d), \quad \text{as } \hat{x}^R \to x^*.$$

To derive a tight confidence set, the asymptotic distribution of $\hat{x}^R$ should be derived. However, it requires strong assumptions on the injury function J, which is not available in some engineering applications. The proof of the three theorems can be found in the appendix.

4.5 Numerical illustration

In this section, we illustrate the proposed method in a hypothetical dataset and then validate the consistency of the point estimator $\hat{x}^R$ and the coverage rate of the interval estimator $\widehat{\mathsf{X}}$. We use univariate responses for simplification. Suppose the true physical process is

$$\zeta(x) = x + 0.003x^4, x \in \mathcal{X} = [-6, 0].$$

The physical tests responses are subject to observational errors $\varepsilon_i \sim N(0, \sigma^2)$ with $\sigma = 0.1$. Assume that the computer model generates responses as

$$\eta(x, \theta) = x + 0.1x^2 + \theta x,$$

with an unknown simulation parameter θ taking values in $[-0.5, 0.5]$. The computer model is not accurate because it misses the x^4 term. An interaction term and a square term are introduced to make a correction. The objective is to find an optimal design to minimize the value of physical responses. The true optimal design can be directly obtained via simple calculus. Its value is $x^* = -4.368$. The procedure of the proposed robust approach is illustrated as four steps in Figure 4.1. First, feasible simulation parameters Θ are selected according to (4.5). Next, the worst-cases are

evaluated in $\Delta(x, \theta)$ for each $\theta \in \Theta$ by assuming the true σ is known. In the third step, the overall worst-cases $\widehat{J}(x)$ are evaluated among all the feasible parameters. Lastly, the robust design $\hat{x}^R$ is searched to minimize the worst-cases $\widehat{J}(x)$.

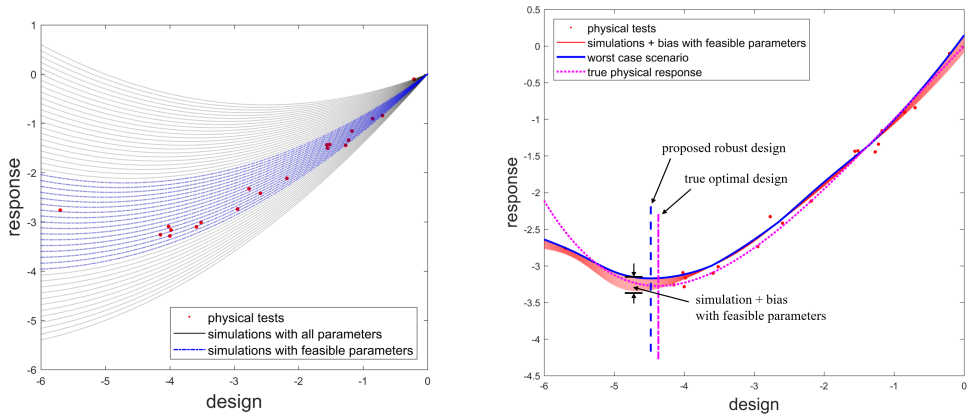

Figure 4.1: Illustration of robust approach. Left panel: 17 out of 51 simulation parameters configurations are selected as feasible simulation parameters. Right panel: the overall worst-case is calculated among all feasible simulation parameters. The proposed robust design is computed based on the worst-case and compared with the true optimal design.

To simulate the randomness, we increase the physical test sample size n from 5 to 50 with step 5. We run 100 iterations of the algorithm for each sample size and then calculate the mean errors and the variances of the solutions from all the iterations. A subset of $\mathcal{X}$ of n samples are randomly drawn and served as the physical test sets in each iteration. The true optimal design x^* always lies within the estimated confidence set for all different sample sizes, showing coverage rates as 1. This result validates the asymptotic coverage rate of 1, implying a loose confidence set. The distribution of $\hat{x}^R$ among all 100 iterations are shown in the box plot in Figure 4.2. It shows the consistency because the bias and variance shrink towards zero as the sample size grows.

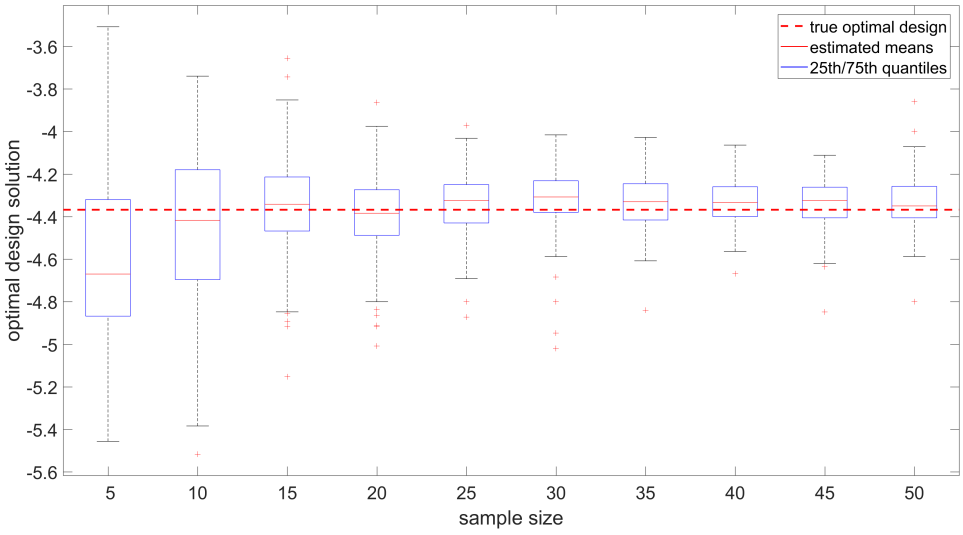

Figure 4.2: Box plot of optimal designs for different sample sizes. The robust designs are compared with the true optimal design to evaluate the performance of the proposed approach. The results are based on 100 replications. The shrinking trend of the bias and variances implies the consistency.

4.6 Case study

We present an analysis of data collected from vehicle crash tests. These tests are conducted with the same dummy under different vehicle design settings. The tests can be simulated by an inexact computer simulation model with additional simulation parameters as inputs. The signals of head accelerations are recorded during the tests. Head Injury Criterion (HIC) value (Eppinger et al., 1999) is used for assessing head safety in each test. It is defined as

$$J(a) = HIC_{15} = \max\{[\frac{1}{t_2 - t_1}\int_{t_1}^{t_2} a(t)dt]^{2.5}(t_2 - t_1)\},$$

where $t_2 - t_1$ is set as 15ms and $a(t)$ is the head acceleration at time t. The objective of this case study is to search for the optimal restraint components design that minimizes the HIC value using the inexact simulation model.

A total of 9 sled tests are included in the physical tests, in which a severe horizontal

crash pulse is applied at the beginning of each test. All tests are conducted with a 5th female adult at the rear seat. The restraint components are intended to engage the occupant early during the crash. It helps absorb the energy with a lower load and avoid the occupant from contacting to the front seat. For the design optimization purpose, 5 different restraint components are studied, which are described as follows:

(a) **Anchor Pretensioner (Anchor PT):** a binary variable about the status of the anchor pretensioner. Enabling it reduces slack in the lap belt.

(b) **Buckle Pretensioner (Buckle PT):** a binary variable about the status of the buckle pretensioner. Enabling it reduces slacks in both the lap and shoulder belts.

(c) **Dynamic Locking Tongue (DLT):** a binary variable on the dynamic locking tongue. Enabling it prevents the lap belt webbing transferring to the shoulder belt (Hu, et al., 2016).

(d) **Load Limiter Type (LLT):** a binary variable showing the type of the load limiter. The load limit force profile can be constant or progressive. A constant load limiter (CLL) provides a constant belt force when the webbing is pulled out. A progressive load limiter (PLL) increases the belt force in contrast in order to limit high excursions toward the end of the impact.

(e) **Torsion Bar (TB):** a continuous variable showing the value of the torsion bar diameter. It is positively correlated to the load limit.

Detailed experiment designs X are shown in Table 4.1.

Accelerations and forces at different body locations are measured by the sensors during the crash tests. Heads are the most important body part and their kinematics during the crash are sensitive to the design of restraint components. Therefore we

Table 4.1: Experiment designs in car crash tests.

Test ID	Occupant	Pulse	Anchor PT	Buckle PT	DLT	LLT	TB
1	5th	Severe	Disabled	Disabled	Disabled	CLL	9.5
2	5th	Severe	Disabled	Disabled	Disabled	PLL	9.5
3	5th	Severe	Disabled	Enabled	Disabled	PLL	9.5
4	5th	Severe	Disabled	Enabled	Disabled	PLL	9.5
5	5th	Severe	Disabled	Enabled	Disabled	CLL	9.5
6	5th	Severe	Disabled	Disabled	Enabled	PLL	10
7	5th	Severe	Disabled	Disabled	Disabled	PLL	10
8	5th	Severe	Enabled	Disabled	Enabled	PLL	10
9	5th	Severe	Disabled	Enabled	Enabled	PLL	10

Table 4.2: Range of simulation parameters.

Simulation parameter	Minimum	Center value	Maximum
Cushion Stiffness	1	1.5	2
Cushion Damping	10	15	20
Cushion Friction	0.8	1.4	2
Initial Strain	-0.15	0.075	0.3

focus on the acceleration at the center of gravity of the head. Head accelerations are recorded as a 1200-length time series with sampling frequency of 100 Hz.

The computer model requires 4 unknown simulation parameters: cushion stiffness, cushion damping, cushion friction and initial strain. All the simulation parameters are considered as continuous variables that are not observable in the physical tests. Their values given in Table 4.2 lie within range based on physical knowledge. It is used to generate Θ based on a Uniform Latin-Hypercube Design (ULHD). A total of 120 possible combinations of simulation parameters are sampled. To compare the simulation responses with physical tests and select feasible simulation parameters, initial simulations are generated with input $X \times \Theta$.

The model bias is estimated based on the kernel regression. Its feasible region is built based on B-spline fitting technique to reduce the dimension of feasible region. We model the time series of bias term by B-spline with 25 basis and determine the values of $\tau_b = 300$ with referring to the domain knowledge. A smaller number of B-spline basis requires more accurate parameters while a greater num-

ber of B-spline basis increases the computation time when calculating the feasible regions. Worst-cases are evaluated among feasible regions of bias for each given simulation parameter. Two illustrative plots of signal profile responses for the 6−th observation are shown in Figure 4.3 where simulation responses $\eta(x_6, \theta)$, physical test responses $y(x_6)$ and simulation responses adding the bias under worst-cases $\eta(x_6, \theta) + \arg\max_{d \in \Delta(x_6,\theta)} J(\eta(x_6, \theta) + d)$ are plotted. On the left panel, the simulation parameters configuration generates a reasonable original simulation response. The simulation signals after adding the bias based on both the kernel regression estimator and the worst-case are compared with the physical test signal. Their differences satisfy the fitting constraint imposed by $\tau_e(x, \theta)$. On the right panel, the simulated response does not follow the pattern shown by the physical test response. Although a bias of $L2$ norm τ_b is added to correct the simulation response, the fitting error still exceeds $\tau_e(x, \theta)$. Consequently, we remove this parameters configuration from the feasible parameters set Θ.

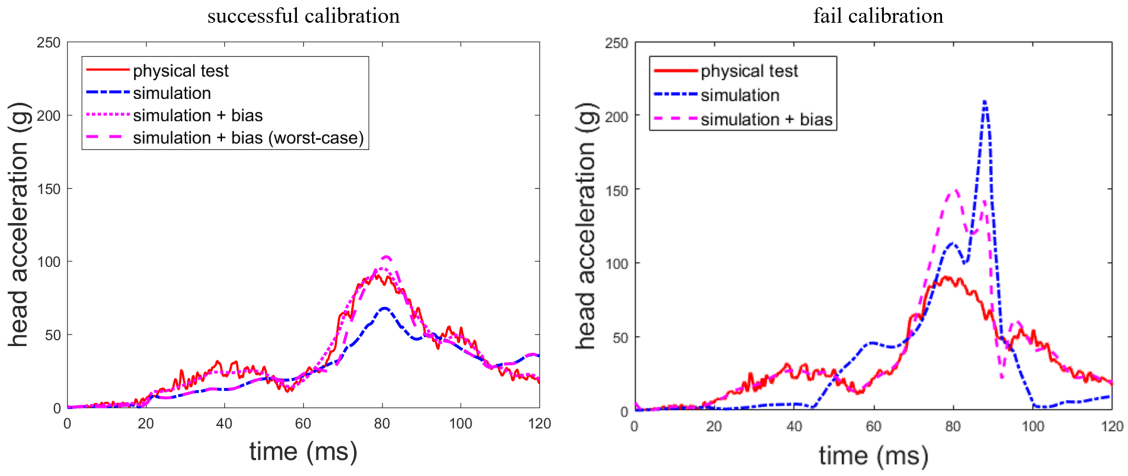

Figure 4.3: Illustrative signal profile responses for a specific experiment setting. Left panel: a simulation response generated from feasible simulation parameters that is calibrated by adding a bias to predict the experiment response. Right panel: a simulation response generated from infeasible simulation parameters which is impossible to be used represent the experiment response by adding a bias satisfying the bias constraint τ_b.

Repeating the above procedure yields a resultant feasible simulation parameter set Θ of 5 elements. Further simulations are generated with inputs from the space $\mathcal{X} \times \Theta$, which is much smaller than the full space. We then construct the feasible region for both the simulation parameter and the bias, then apply robust optimization approach. The robust optimization approach suggests an optimal design with $(Enabled, Disabled, Enabled, CLL, 10)$. Based on the domain knowledge, it makes use of the advanced belt design, which can avoid head contact and reduce the crash impact to the human body with a relatively low TB. To make a comparison with the existing method, we fix the simulation parameters as the center values θ_0 shown in Table 4.2 and search for the optimal design by minimizing the simulated injury values. Then we sort the worst-cases $\widehat{J}(x)$ and compare them with the corresponding simulated injury values $J\left(\eta(x, \theta_0)\right)$. The simulated injury values show an overall decreasing trend in Figure 4.4 with non-monotonous patterns at some of the designs. This implies that the proposed method captures the overall trend of simulation responses and makes adjustment to the responses corresponding to certain regions of the design space. The computer simulation model generates an optimal design with $(Disabled, Disabled, Disabled, PLL, 11)$, which does not agree with the proposed method. This design prevents the body damage by a maximal TB without using most of the advanced belt designs. It is considered less reliable than the optimal design provided by the proposed method based on the domain knowledge.

4.7 Discussion

In this paper, we present a method to search for the optimal system design using an inexact computer simulation model with uncertainty. The uncertainty is quantified by feasible regions instead of building a full probabilistic model, which makes the

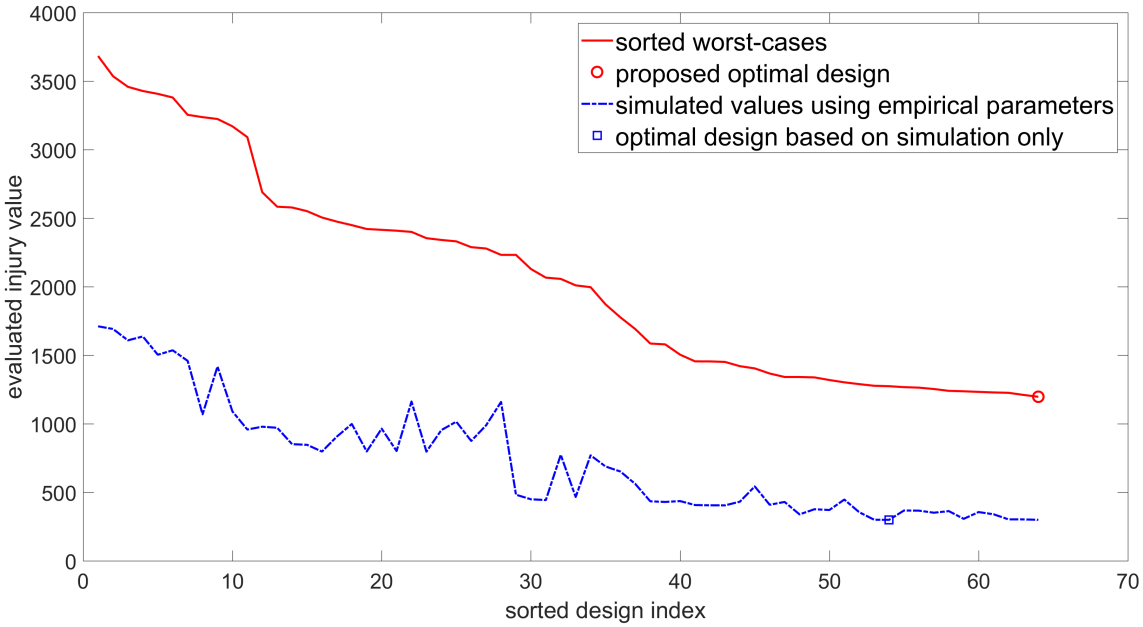

Figure 4.4: Comparison between optimal designs obtained from the proposed method and the existing method. The sorted $\widehat{J}(x)$ are compared with $J\left(\eta(x,\theta_0)\right)$ generated from corresponding designs. The optimal designs labeled as circle and square reflect the differences of the two methods.

proposed method to be applicable when an emulator is not available. The use of feasible regions also narrow the potential simulation parameter set and reduces the computation load in generating simulation runs. A robust optimization problem is formulated and integrated with the model calibration, which is solved based on the feasible regions to generate the simulations. The proposed point and interval estimators of the optimal design are mathematically proved to have consistency and coverage properties.

In this paper, Kernel smoothing is used to estimate the model bias in the full design space $\mathcal{X}$. It guarantees the uniform consistency at a rate of $O_p\left(\left(\frac{\ln n}{n}\right)^{2/(q+4)}\right)$. An alternative is to apply Gaussian process modeling or any other non-parametric approaches to estimate the model bias. These alternative approaches may give some other convergence rates. Theoretical research in optimizing the convergence rate is

expected. In addition, the confidence set has a coverage rate of 1 as n goes to infinity. To obtain a tighter confidence set, further efforts are required to calculate the inverse of Jacobian of $\widehat{J}(x)$ and then obtain the asymptotic distribution of $\hat{x}^R$ from that of $\widehat{J}(x)$. A prerequisite is to assume $J \in C^1$ instead of the Lipschitz continuity in Assumption 5.

The objective function J is maximized with respect to the simulation parameters and the model bias in the robust optimization step and then used for comparing different designs. In the vehicle design application, simulation parameters are considered as random variables that may take different values at different design configurations. Therefore we evaluate the worst-case for each given parameters configurations then maximize J in the feasible parameters set Θ. However, in some other applications, simulation parameters take fixed values that need to be estimated. In this case, all physical experiments are supposed to share the same simulation parameters. It is desired to find a uniform simulation parameter to conduct the comparisons. A natural implementation is to search for a combination of simulation parameters at the first step. Then the optimal design is searched based on the determined simulation parameters.

4.8 Proof of Theorems

To begin with, we restate the Theorem 2 of Hansen (2008) for uniform consistency of the Kernel regression estimator for a univariate response. It gives a convergence rate of $O_p\left(\left(\frac{\ln n}{n}\right)^{2/(q+4)}\right)$ when $h_j = Cn^{-1/(q+4)}$.

Lemma 1 (Hansen, 2008): Let $\tilde{\delta}_{n,j}(x,\theta)$ and $\delta_j(x,\theta)$ denote the j-th dimension of vector $\tilde{\delta}_n(x,\theta)$ and $\delta(x,\theta)$, respectively. Under Assumptions 1-5, for some $C < \infty$, the following uniform consistency holds:

$$\sup_{\|x\| \leq C} \left|\tilde{\delta}_{n,j}(x,\theta) - \delta_j(x,\theta)\right| = O_p\left(\left(\frac{\ln n}{n}\right)^{2/(q+4)}\right).$$

Now we extend the uniform consistency for univariate responses to that for multivariate responses by assuming the independence between different dimensions in Assumption 6.

Lemma 2: Under Assumptions 1-6, for some $C < \infty$, the following uniform consistency holds:

$$\sup_{\|x\| \leq C} \left\|\tilde{\delta}_n(x,\theta) - \delta(x,\theta)\right\| = O_p\left(\left(\frac{\ln n}{n}\right)^{2/(q+4)}\right).$$

Proof of Lemma 2. Lemma 1 implies that for any $\varepsilon > 0$, there exist $M_1, ..., M_L$, such that

$$\mathbb{P}\left[\frac{\sup_{\|x\| \leq C}\left|\tilde{\delta}_{n,j}(x,\theta) - \delta_j(x,\theta)\right|}{\left(\frac{\ln n}{n}\right)^{2/(q+4)}} \leq M_j\right] \geq \varepsilon^{1/L}, \text{ for any } j \in \{1, ..., L\}. \qquad \text{(A1)}$$

Let $M = \sqrt{\sum_{j=1}^{L} M_j^2}$. By (A1) and Assumption 6:

$$
\begin{aligned}
&\mathbb{P}\left[\frac{\sup_{\|x\|\leq C}\left\|\tilde{\delta}_{n,j}(x,\theta)-\delta_j(x,\theta)\right\|}{\left(\frac{\ln n}{n}\right)^{2/(q+4)}} \leq M\right] \\
&\geq \mathbb{P}\left[\frac{\sup_{\|x\|\leq C}\left\|\tilde{\delta}_{n,1}(x,\theta)-\delta_1(x,\theta)\right\|}{\left(\frac{\ln n}{n}\right)^{2/(q+4)}} \leq M_1, ..., \frac{\sup_{\|x\|\leq C}\left\|\tilde{\delta}_{n,L}(x,\theta)-\delta_L(x,\theta)\right\|}{\left(\frac{\ln n}{n}\right)^{2/(q+4)}} \leq M_L\right] \\
&= \prod_{j=1}^{L} \mathbb{P}\left[\frac{\sup_{\|x\|\leq C}\left\|\tilde{\delta}_{n,j}(x,\theta)-\delta_j(x,\theta)\right\|}{\left(\frac{\ln n}{n}\right)^{2/(q+4)}} \leq M_j\right] \\
&\geq \prod_{j=1}^{L} \varepsilon^{1/L} \\
&= \varepsilon,
\end{aligned}
$$

which is the formal definition of the uniform consistency

$$\sup_{\|x\|\leq C}\left\|\tilde{\delta}_n(x,\theta)-\delta(x,\theta)\right\| = O_p\left(\left(\frac{\ln n}{n}\right)^{2/(q+4)}\right).$$

Proof of Theorem 1. We first show the uniform consistency

$$\sup_{x\in\mathcal{X}}\left|\widehat{J}(x)-J(\zeta(x))\right| \to_p 0, \text{ as } n\to\infty.$$

then prove the consistency of $\hat{x}^R$. By Assumption 7, for any $y_1, y_2 \in \mathbb{R}^L$, $|J(y_1) - J(y_2)| \leq \Lambda_2 \|y_1 - y_2\|$. Then for any $\theta \in \Theta$,

$$\begin{aligned}
&\left|\widehat{J}(x) - J(\zeta(x))\right| \\
&= \left|\widehat{J}(x) - J(\eta(x,\theta) + \tilde{\delta}_n(x,\theta)) + J(\eta(x,\theta) + \tilde{\delta}_n(x,\theta)) - J(\eta(x,\theta) + \delta(x,\theta))\right| \\
&\leq \left|\widehat{J}(x) - J(\eta(x,\theta) + \tilde{\delta}_n(x,\theta))\right| + \left|J(\eta(x,\theta) + \tilde{\delta}_n(x,\theta)) - J(\eta(x,\theta) + \delta(x,\theta))\right| \\
&\leq \left|\widehat{J}(x) - J(\eta(x,\theta) + \tilde{\delta}_n(x,\theta))\right| + \Lambda_2 \left\|\tilde{\delta}_n(x,\theta) - \delta(x,\theta)\right\| \\
&\leq \Lambda_2 \left\|\arg\max_{d \in \Delta(x,\theta)} J(\eta(x,\theta) + d) - \tilde{\delta}_n(x,\theta)\right\| + \Lambda_2 \left\|\tilde{\delta}_n(x,\theta) - \delta(x,\theta)\right\| \\
&\leq \Lambda_2 \tau_e(x,\theta) + \Lambda_2 \left\|\tilde{\delta}_n(x,\theta) - \delta(x,\theta)\right\| \\
&= O_p\left(\left(\frac{1}{n}\right)^{2/(q+4)}\right) + O_p\left(\left(\frac{\ln n}{n}\right)^{2/(q+4)}\right) \\
&= O_p\left(\left(\frac{\ln n}{n}\right)^{2/(q+4)}\right).
\end{aligned}$$

Thus we have

$$\sup_{x \in \mathcal{X}} \left|\widehat{J}(x) - J(\zeta(x))\right| \to_p 0.$$

Next, we want to show that $\hat{x}^R \to_p x^*$. Note that Assumption 8 yields

$$\mathbb{P}\left[\left\|\hat{x}^R - x^*\right\| > \varepsilon\right] \leq \mathbb{P}\left[J(\zeta(\hat{x}^R)) - J(\zeta(x^*)) > \tau\right].$$

It implies that the result would follow after showing that $J(\zeta(\hat{x}^R)) - J(\zeta(x^*)) = o_p(1)$. To see this, notice that $\widehat{J}(\hat{x}^R) \geq \widehat{J}(x^*) - o_p(1)$ is given by Assumption 9, and therefore

$$\begin{aligned}
&J(\zeta(\hat{x}^R)) - J(\zeta(x^*)) \\
&\leq \left|J(\zeta(\hat{x}^R)) - \widehat{J}(\hat{x}^R)\right| + \left|\widehat{J}(\hat{x}^R) - \widehat{J}(x^*)\right| + \left|\widehat{J}(x^*) - J(\zeta(x^*))\right| \\
&\leq 2 \sup_{x \in \mathcal{X}} \left|J(\zeta(x)) - \widehat{J}(x)\right| + o_p(1) \\
&= o_p(1),
\end{aligned}$$

giving the result.

To calculate $\mathbb{P}\left[\widehat{J}(x) \geq J(\zeta(x))\right]$, we need to know the asymptotic distribution of $\eta(x,\theta) + \tilde{\delta}_n(x,\theta)$ first. Härdle and Müller (1997) and Ruppert and Wand (1994) derived the asymptotic distribution of the Kernel regression estimator. The following lemma is rewritten based on the Theorem 1 in Härdle and Müller (1997).

Lemma 3 (Härdle and Müller, 1997): Suppose Assumptions 1-5 and Assumption 10 hold, let $\delta_j(x,\theta)$ denote the j-th element of the vector $\delta(x,\theta)$ and x_j denote the j-th element of the vector x. Then

$$\sqrt{nh_1...h_q}\left(\tilde{\delta}_{n,j}(x,\theta) - \delta_j(x,\theta) - B_j(x,\theta)\right) \to_d N\left(0, \frac{R(k)^q\sigma^2}{f(x)}\right),$$

where

$$B_j(x,\theta) = \kappa_2 \sum_{j=1}^{q} h_j^2 \left[\frac{1}{2}\frac{\partial^2}{\partial x_j^2}\delta_j(x,\theta) + f(x)^{-1}\frac{\partial}{\partial x_j}\delta_j(x,\theta)\frac{\partial}{\partial x_j}f(x)\right],$$

$$R(k) = \int k(u)^2 du,$$

$$\kappa_2 = \int k(u)u^2 du.$$

Therefore the asymptotic distribution of $\tilde{\delta}_n(x,\theta)$ can be directly obtained from the asymptotic distribution of its each dimension by adding Assumption 3.

Lemma 4: Under Assumptions 1-6 and Assumption 10,

$$\sqrt{nh_1...h_q}\left(\tilde{\delta}_n(x,\theta) - \delta(x,\theta) - B(x,\theta)\right) \to_d N\left(0, \frac{R(k)^q\sigma^2}{f(x)}I_L\right),$$

where $B(x,\theta) = \{B_1(x,\theta), ..., B_L(x,\theta)\}$.

Next, we calculate the probability that the true bias $\delta(x,\theta)$ satisfies the fitting accuracy constraint $\left\|d - \tilde{\delta}_n(x,\theta)\right\| \leq \tau_e(x,\theta)$. Since σ is not available in some applications, we use the estimates in Fan and Yao (1998) instead.

Lemma 5: Under Assumptions 1-6 and Assumption 10,

$$\mathbb{P}\left[\left\|\delta(x,\theta) - \tilde{\delta}_n(x,\theta)\right\| \leq \tau_e(x,\theta)\right] \to 1-\alpha, \quad n \to \infty,$$

where

$$\tau_e(x,\theta) = \sqrt{\chi^2_{L,1-\alpha}\frac{R_k^q\hat{\sigma}^2(\theta)}{\hat{f}(x)}},$$

$$\hat{\sigma}^2(\theta) = \frac{1}{n-1}\sum_{i=1}^{n}(y_i - \eta(x_i,\theta) - \tilde{\delta}_n(x_i,\theta))^2,$$

$$\hat{f}(x) = \sum_{i=1}^{n} K(H^{-1}(x_i - x)).$$

Proof of Lemma 5. To begin with, we write $\tilde{\delta}_n(x,\theta) - \delta(x,\theta) - B(x,\theta)$'s asymptotic covariance matrix as:

$$\mathbb{C}\text{ov}\left[\tilde{\delta}_n(x,\theta) - \delta(x,\theta) - B(x,\theta)\right] = \frac{R(k)^q\sigma^2}{nh_1...h_q f(x)} I_L.$$

Therefore the squared $L2$ norm of $\tilde{\delta}_n(x,\theta) - \delta(x,\theta)$ follows χ^2 distribution with L degrees of freedom. Its $100(1-\alpha)\%$-th quantile is used to set the constraint in the optimization step as:

$$\mathbb{P}\left[\left\|\tilde{\delta}_n(x,\theta) - \delta(x,\theta) - B(x,\theta)\right\| \leq \sqrt{\chi^2_{L,1-\alpha}\frac{R(k)^q\sigma^2}{nh_1...h_q f(x)}}\right] = 1-\alpha.$$

Now we use the estimates of $f(x)$ and σ^2 in Fan and Yao (1998) and consider the limit of $B(x,\theta)$.

$$\hat{\sigma}^2(\theta) \to_p \sigma^2, \text{ for any } \theta, \tag{A2}$$

$$\hat{f}(x) \to_p f(x), \tag{A3}$$

$$B(x,\theta) \to_p 0.$$

Let $\tau_e(x,\theta) = \sqrt{\frac{R(k)^q\sigma^2}{nh_1...h_q f(x)}}$ and $\hat{\tau}_e(x,\theta) = \sqrt{\frac{R(k)^q\hat{\sigma}^2(\theta)}{nh_1...h_q\hat{f}(x)}}$. Combining (A2) and (A3) yields:

$$\hat{\tau}_e(x,\theta) \to_p \tau_e(x,\theta).$$

Next, we are going to show that:

$$\mathbb{P}\left[\left\|\tilde{\delta}_n(x,\theta) - \delta(x,\theta)\right\| \leq \tau_e(x,\theta)\right] \to 1-\alpha.$$

As $B(x,\theta) \to_p 0$, for any $\nu, \epsilon > 0$, there exists h^*, such that when $\max\{h_1, ..., h_q\} < h^*$,

$$\mathbb{P}\left[\|B(x,\theta)\| > \nu\right] \leq \epsilon.$$

By triangular inequality,

$$\begin{aligned}
&\mathbb{P}\left[\left\|\tilde{\delta}_n(x,\theta) - \delta(x,\theta) - B(x,\theta)\right\| + \|B(x,\theta)\| \leq \tau_e(x,\theta)\right] \\
\leq\ &\mathbb{P}\left[\left\|\tilde{\delta}_n(x,\theta) - \delta(x,\theta)\right\| \leq \tau_e(x,\theta)\right] \\
\leq\ &\mathbb{P}\left[\left\|\tilde{\delta}_n(x,\theta) - \delta(x,\theta) - B(x,\theta)\right\| - \|B(x,\theta)\| \leq \tau_e(x,\theta)\right].
\end{aligned}$$

We want to derive the limits of the lower and upper bounds in the above inequality and then apply the squeeze theorem. For the lower bound,

$$\begin{aligned}
&\mathbb{P}\left[\left\|\tilde{\delta}_n(x,\theta) - \delta(x,\theta)\right\| \leq \tau_e(x,\theta)\right] \\
\leq\ &\mathbb{P}\left[\left\|\tilde{\delta}_n(x,\theta) - \delta(x,\theta) - B(x,\theta)\right\| - \|B(x,\theta)\| \leq \tau_e(x,\theta)\right] \\
=\ &\mathbb{P}\left[\left\|\tilde{\delta}_n(x,\theta) - \delta(x,\theta) - B(x,\theta)\right\| - \|B(x,\theta)\| \leq \tau_e(x,\theta) \,\middle|\, \|B(x,\theta)\| \leq \nu\right] \\
&\times \mathbb{P}\left[\|B(x,\theta)\| \leq \nu\right] \\
&+ \mathbb{P}\left[\left\|\tilde{\delta}_n(x,\theta) - \delta(x,\theta) - B(x,\theta)\right\| - \|B(x,\theta)\| \leq \tau_e(x,\theta) \,\middle|\, \|B(x,\theta)\| > \nu\right] \\
&\times \mathbb{P}\left[\|B(x,\theta)\| > \nu\right] \\
\leq\ &\mathbb{P}\left[\left\|\tilde{\delta}_n(x,\theta) - \delta(x,\theta) - B(x,\theta)\right\| \leq \tau_e(x,\theta) + \nu\right](1-\epsilon) \\
&+ \mathbb{P}\left[\left\|\tilde{\delta}_n(x,\theta) - \delta(x,\theta) - B(x,\theta)\right\| - \|B(x,\theta)\| \leq \tau_e(x,\theta) \,\middle|\, \|B(x,\theta)\| > \nu\right] \\
&\times \mathbb{P}\left[\|B(x,\theta)\| > \nu\right] \\
\to\ &\mathbb{P}\left[\left\|\tilde{\delta}_n(x,\theta) - \delta(x,\theta) - B(x,\theta)\right\| \leq \tau_e(x,\theta)\right], \quad \epsilon, \nu \to 0.
\end{aligned}$$

For the upper bound,

$$
\begin{aligned}
&\mathbb{P}\left[\left\|\tilde{\delta}_n(x,\theta)-\delta(x,\theta)\right\| \le \tau_e(x,\theta)\right] \\
&\ge \mathbb{P}\left[\left\|\tilde{\delta}_n(x,\theta)-\delta(x,\theta)-B(x,\theta)\right\| + \|B(x,\theta)\| \le \tau_e(x,\theta)\right] \\
&= \mathbb{P}\left[\left\|\tilde{\delta}_n(x,\theta)-\delta(x,\theta)-B(x,\theta)\right\| + \|B(x,\theta)\| \le \tau_e(x,\theta)\,\middle|\, \|B(x,\theta)\| \le \nu\right] \\
&\times \mathbb{P}\left[\|B(x,\theta)\| \le \nu\right] \\
&+ \mathbb{P}\left[\left\|\tilde{\delta}_n(x,\theta)-\delta(x,\theta)-B(x,\theta)\right\| + \|B(x,\theta)\| \le \tau_e(x,\theta)\,\middle|\, \|B(x,\theta)\| > \nu\right] \\
&\times \mathbb{P}\left[\|B(x,\theta)\| > \nu\right] \\
&\ge \mathbb{P}\left[\left\|\tilde{\delta}_n(x,\theta)-\delta(x,\theta)-B(x,\theta)\right\| \le \tau_e(x,\theta)-\nu\right](1-\epsilon) \\
&+ \mathbb{P}\left[\left\|\tilde{\delta}_n(x,\theta)-\delta(x,\theta)-B(x,\theta)\right\| + \|B(x,\theta)\| \le \tau_e(x,\theta)\,\middle|\, \|B(x,\theta)\| > \nu\right] \\
&\times \mathbb{P}\left[\|B(x,\theta)\| > \nu\right] \\
&\to \mathbb{P}\left[\left\|\tilde{\delta}_n(x,\theta)-\delta(x,\theta)-B(x,\theta)\right\| \le \tau_e(x,\theta)\right], \quad \epsilon,\nu \to 0.
\end{aligned}
$$

By the squeeze theorem, we have

$$
\begin{aligned}
&\mathbb{P}\left[\left\|\tilde{\delta}_n(x,\theta)-\delta(x,\theta)\right\| \le \tau_e(x,\theta)\right] \\
&\to \mathbb{P}\left[\left\|\tilde{\delta}_n(x,\theta)-\delta(x,\theta)-B(x,\theta)\right\| \le \tau_e(x,\theta)\right].
\end{aligned}
$$

Similarly, we can show that

$$
\mathbb{P}\left[\left\|\tilde{\delta}_n(x,\theta)-\delta(x,\theta)\right\| \le \tau_e(x,\theta)\right] \to \mathbb{P}\left[\left\|\tilde{\delta}_n(x,\theta)-\delta(x,\theta)\right\| \le \hat{\tau}_e(x,\theta)\right].
$$

In summary, we have

$$
\begin{aligned}
&\mathbb{P}\left[\left\|\tilde{\delta}_n(x,\theta)-\delta(x,\theta)\right\| \le \tau_e(x,\theta)\right] \\
&\to \mathbb{P}\left[\left\|\tilde{\delta}_n(x,\theta)-\delta(x,\theta)-B(x,\theta)\right\| \le \hat{\tau}_e(x,\theta)\right] \\
&= 1-\alpha.
\end{aligned}
$$

Proof of Theorem 2. Lemma 5 implies that $\mathbb{P}[\delta(x,\theta) \in \Delta(x,\theta)] \to 1-\alpha$. Therefore

$$\begin{aligned}
&\mathbb{P}\left[\widehat{J}(x) \geq J(\zeta(x))\right] \\
&= \mathbb{P}\left[\max_{d\in\Delta(x,\theta)} J(\eta(x,\theta)+d) \geq J(\eta(x,\theta)+\delta(x,\theta))\right] \\
&\geq \mathbb{P}\left[\delta(x,\theta) \in \Delta(x,\theta)\right] \\
&\to 1-\alpha.
\end{aligned}$$

Proof of Theorem 3.

Theorem 1 guarantees that $\widehat{J}(x)$ converges to $J(\zeta(x))$ uniformly, which yields

$$\widehat{J}(\hat{x}^R) \to_p J(\zeta(\hat{x}^R)), n \to \infty,$$

$$\widehat{J}(x^*) \to_p J(\zeta(x^*)), n \to \infty.$$

Also we know that $\hat{x}^R \to_p x^*$, by Assumption 7,

$$J(\zeta(\hat{x}^R)) \to_p J(\zeta(x^*)).$$

Combining the above three limiting equalities together yields

$$\widehat{J}(\hat{x}^R) \to_p \widehat{J}(x^*).$$

Now we derive $\mathbb{P}\left[x^* \in \widehat{\mathsf{X}}\right]$ based on the definition of $\widehat{\mathsf{X}}$.

$$\begin{aligned}
&\mathbb{P}\left[x^* \in \widehat{\mathsf{X}}\right] \\
&= \mathbb{P}\left[\min_{d\in\Delta(x^*,\theta)} J(\eta(x^*,\theta)+d) \leq \max_{d\in\Delta(\hat{x}^R,\theta)} J(\eta(\hat{x}^R,\theta)+d)\right] \\
&\to \mathbb{P}\left[\min_{d\in\Delta(x^*,\theta)} J(\eta(x^*,\theta)+d) \leq \max_{d\in\Delta(x^*,\theta)} J(\eta(x^*,\theta)+d)\right] \\
&= 1 \geq 1-\alpha.
\end{aligned}$$

CHAPTER V

Conclusions and Future Research

5.1 Conclusions

This dissertation presents new methodologies to quantify the uncertainties of functional data for the purpose of vehicle safety evaluation and design optimization in biomechanical applications. A new method for developing confidence bands for univariate functional signal responses is firstly presented. The resultant confidence bands take subject variables into consideration. Then a generic methodology is developed to build confidence bands for bivariate functional signal responses with a complicated covariance structure. Lastly, a robust design optimization approach is developed to integrate the responses from an inexact computer simulation model and limited physical tests. The main research results and new contributions of this dissertaion are summarized as follows:

(1) Confidence band construction for univariate functional signal responses based on principal component analysis. An effective method is developed for confidence bands generation that applies principal component analysis (PCA). Rather than using existing empirical models to account for the effects of subject variables on functional responses, linear regression models are further built to model the relationship between extracted PC features and subject variables, which makes the effects of subject variables interpretable. The advantage of the resultant

confidence bands is reflected by the narrower bands than those generated by existing techniques while keeping a high coverage rate of sampled experimental functional data.

(2) Confidence band development for bivariate functional signal responses using Gaussian process modeling. The effect of subject variables is quantified by non-parametric B-spline fitting and a polynomial regression model, which is capable of capturing non-linear dependencies between the subject variables and functional responses. Moreover, a Gaussian process model is developed to model the complicated covariance structure, which can fully consider between-subjects and within-subject variability, auto-correlation between time points and cross-correlation between two responses. Therefore, the constructed confidence bands can effectively capture the bivariate functional profile shape and functional variation patterns. As a byproduct, the developed model is effectively used for testing outliers of abnormal functional responses based on the property of the developed Gaussian process model.

(3) Robust system design optimization with limited experimental data and an inexact simulation model. A method to search for the optimal system design using an inexact computer simulation model with uncertainty quantification is developed. The uncertainty is quantified by specifying feasible regions instead of building a full probabilistic model, which makes the proposed method to be applicable when an emulator is not available. The use of feasible regions also narrow the potential simulation parameter set and reduces the computation load in generating simulation runs. An robust optimization problem is formulated and integrated with the model calibration. The proposed point and interval estimators of the optimal design are mathematically proved to have consistency and coverage properties.

5.2 Future research

In this dissertation, some research has been conducted and demonstrated in both methodology developments and biomechanical applications. However, future research is expected in this area, and a few examples of such research topics are listed below.

- Continue to the confidence band construction problem, it is desired to construct confidence bands for multivariate functional signal responses. The cross-correlations between multivariate signals should be modeled. This can be generally extended to monitor the cross-correlations between multiple signals in broad manufacturing applications.
- In the computer model calibration problem, multivariate functional signal responses will be considered in the uncertainty quantification. Moreover, the physical tests that record functional responses are expensive. However, the daily system operational data are easier to collect from real applications. For example, in vehicle design applications, it is more convenient to collect a binary response showing whether the driver is injured or not during accidents. This can further increase the sample size of system responses with a low resolution. Future research will be explored how to integrate these low resolution data with high resolution computer simulation data for system design optimization.
- In the computer model calibration problem, most of the safety evaluation experiments and simulations focus on a mid-size male or female, which cannot represent the whole population. A more comprehensive model that predicts subject responses for all possible combinations of vehicle designs and subject variables can be established when more experimental or simulation data are available.

In this case, it is of researchers' interests to optimize the vehicle design for a certain subgroup of population. The optimization and grouping techniques that provide personalized vehicle designs have not yet been explored.

BIBLIOGRAPHY

Bruce Ankenman, Barry L Nelson, and Jeremy Staum. Stochastic kriging for simulation metamodeling. *Operations research*, 58(2):371–382, 2010.

Kristy B Arbogast, Sriram Balasubramanian, Thomas Seacrist, Matthew R Maltese, J Felipe Garcia-Espana, Terrence Hopely, Eric Constans, Francisco J López-Valdés, Richard W Kent, Hiromasa Tanji, et al. Comparison of kinematic responses of the head and spine for children and adults in low-speed frontal sled tests. Technical report, SAE Technical Paper, 2009.

MJ Bayarri, JO Berger, John Cafeo, G Garcia-Donato, F Liu, J Palomo, RJ Parthasarathy, R Paulo, Jerry Sacks, D Walsh, et al. Computer model validation with functional output. *The Annals of Statistics*, 35(5):1874–1906, 2007.

E Bektas, K Broermann, G Pećanac, S Rzepka, C Silber, and B Wunderle. Robust design optimization: On methodology and short review. In *Thermal, Mechanical and Multi-Physics Simulation and Experiments in Microelectronics and Microsystems (EuroSimE), 2017 18th International Conference on*, pages 1–7. IEEE, 2017.

Xiaoguang Chen, Timothy Hasselman, Douglas Neill, Xiaoguang Chen, Timothy Hasselman, and Douglas Neill. Reliability based structural design optimization for practical applications. In *38th Structures, structural dynamics, and materials conference*, page 1403, 1997.

Ioannis Doltsinis and Zhan Kang. Robust design of structures using optimization

methods. *Computer methods in applied mechanics and engineering*, 193(23-26): 2221–2237, 2004.

Bruce R Donnelly and Kevin Moorhouse. Optimized phasing of pmhs response curves for biofidelity targets. In *IRCOBI Conference Proceedings*, number IRC-12-51, 2012.

Bruce R Donnelly, Kevin M Moorhouse, Heather H Rhule, and Jason A Stammen. A deformation energy approach to normalizing pmhs response data and developing biofidelity targets for dummy design. In *Proceedings of IRCOBI Conference*, 2014.

I Enevoldsen and John Dalsgaard Sørensen. Reliability-based optimization in structural engineering. *Structural safety*, 15(3):169–196, 1994.

Rolf Eppinger, Emily Sun, Faris Bandak, Mark Haffner, Nopporn Khaewpong, Matt Maltese, Shashi Kuppa, Thuvan Nguyen, Erik Takhounts, Rabih Tannous, et al. Development of improved injury criteria for the assessment of advanced automotive restraint systems–ii. *National Highway Traffic Safety Administration*, pages 1–70, 1999.

Rolf H Eppinger, Jeffrey H Marcus, and Richard M Morgan. Development of dummy and injury index for nhtsa's thoracic side impact protection research program. Technical report, SAE Technical Paper, 1984.

Jianqing Fan and Qiwei Yao. Efficient estimation of conditional variance functions in stochastic regression. *Biometrika*, 85(3):645–660, 1998.

Marian Farah, Paul Birrell, Stefano Conti, and Daniela De Angelis. Bayesian emulation and calibration of a dynamic epidemic model for a/h1n1 influenza. *Journal of the American Statistical Association*, 109(508):1398–1411, 2014.

FS Gayzik, IP Marcus, KA Danelson, JD Rupp, CR Bass, N Yoganandan, and J Zhang. A point-wise normalization method for development of biofidelity response corridors. *Journal of biomechanics*, 48(15):4173–4177, 2015.

Tilmann Gneiting, Marc G Genton, and Peter Guttorp. Geostatistical space-time models, stationarity, separability, and full symmetry. *Monographs On Statistics and Applied Probability*, 107:151, 2006.

Robert B Gramacy, Derek Bingham, James Paul Holloway, Michael J Grosskopf, Carolyn C Kuranz, Erica Rutter, Matt Trantham, R Paul Drake, et al. Calibrating a large computer experiment simulating radiative shock hydrodynamics. *The Annals of Applied Statistics*, 9(3):1141–1168, 2015.

Bruce E Hansen. Uniform convergence rates for kernel estimation with dependent data. *Econometric Theory*, 24(3):726–748, 2008.

Wolfgang Härdle and Marlene Müller. Multivariate and semiparametric kernel regression. Technical report, Discussion Papers, Interdisciplinary Research Project 373: Quantification and Simulation of Economic Processes, 1997.

Trevor Hastie, Robert Tibshirani, and Martin Wainwright. *Statistical learning with sparsity: the lasso and generalizations*. CRC press, 2015.

Dave Higdon, James Gattiker, Brian Williams, and Maria Rightley. Computer model calibration using high-dimensional output. *Journal of the American Statistical Association*, 103(482):570–583, 2008.

Jingwen Hu, Jun Wu, Kathleen D Klinich, Matthew P Reed, Jonathan D Rupp, and Libo Cao. Optimizing the rear seat environment for older children, adults, and infants. *Traffic injury prevention*, 14(sup1):S13–S22, 2013.

Jingwen Hu, Kurt Fischer, Paul Lange, and Angelo Adler. Effects of crash pulse, impact angle, occupant size, front seat location, and restraint system on rear seat occupant protection. Technical report, SAE Technical Paper, 2015.

Peter J Huber. Robust statistics. In *International Encyclopedia of Statistical Science*, pages 1248–1251. Springer, 2011.

Gareth M James et al. Curve alignment by moments. *The Annals of Applied Statistics*, 1(2):480–501, 2007.

Hector A Jensen. Structural optimization of non-linear systems under stochastic excitation. *Probabilistic Engineering Mechanics*, 21(4):397–409, 2006.

Marc C Kennedy and Anthony O'Hagan. Bayesian calibration of computer models. *Journal of the Royal Statistical Society: Series B (Statistical Methodology)*, 63(3): 425–464, 2001.

DE Kinser and F Moses. Optimum structural design with failure probability constraints. *AIAA Journal*, 5(6):1152–1158, 1967.

Kwon-Hee Lee and Gyung-Jin Park. Robust optimization considering tolerances of design variables. *Computers & Structures*, 79(1):77–86, 2001.

TE Lobdell, CK Kroell, DC Schneider, WE Hering, and AM Nahum. Impact response of the human thorax. In *Human Impact Response*, pages 201–245. Springer, 1973.

Matthew R Maltese, Rolf H Eppinger, Heather H Rhule, Bruce R Donnelly, Frank A Pintar, and Narayan Yoganandan. Response corridors of human surrogates in lateral impacts. Technical report, SAE Technical Paper, 2002.

Harold J Mertz. A procedure for normalizing impact response data. Technical report, SAE Technical Paper, 1984a.

Harold J Mertz. A procedure for normalizing impact response data. Technical report, SAE Technical Paper, 1984b.

Kevin Moorhouse et al. An improved normalization methodology for developing mean human response curves. In *Proceedings of the International Conference of Enhanced Safety of Vehicles, Seoul, Korea, Paper*, number 13-0192, 2013.

Elizbar A Nadaraya. On estimating regression. *Theory of Probability & Its Applications*, 9(1):141–142, 1964.

Guy S Nusholtz, Zine Aoun, Laura Di Domenico, Timothy Hsu, Manuel A Gracián, and Jesús A Prado. Statistical considerations for evaluating biofidelity, repeatability, and reproducibility of atds. *SAE International journal of transportation safety*, 1(1):200–218, 2013.

Matthew Plumlee. Bayesian calibration of inexact computer models. *Journal of the American Statistical Association*, 112(519):1274–1285, 2017.

Matthew Plumlee, V Roshan Joseph, and Hui Yang. Calibrating functional parameters in the ion channel models of cardiac cells. *Journal of the American Statistical Association*, 111(514):500–509, 2016.

Carl Edward Rasmussen and Christopher KI Williams. *Gaussian process for machine learning*. MIT press, 2006.

BD Ripley. Modern applied statistics with s. *Statistics and Computing, fourth ed. Springer, New York*, 2002.

David Ruppert and Matthew P Wand. Multivariate locally weighted least squares regression. *The annals of statistics*, pages 1346–1370, 1994.

Gerhart I Schuëller and Hector A Jensen. Computational methods in optimization considering uncertainties–an overview. *Computer Methods in Applied Mechanics and Engineering*, 198(1):2–13, 2008.

W Sun, JH Jin, MP Reed, FS Gayzik, KA Danelson, CR Bass, JY Zhang, and JD Rupp. A method for developing biomechanical response corridors based on principal component analysis. *Journal of biomechanics*, 49(14):3208–3215, 2016.

Genichi Taguchi. Introduction to quality engineering: designing quality into products and processes. Technical report, 1986.

Rui Tuo, CF Jeff Wu, et al. Efficient calibration for imperfect computer models. *The Annals of Statistics*, 43(6):2331–2352, 2015.

Marcos A Valdebenito and Gerhart I Schuëller. A survey on approaches for reliability-based optimization. *Structural and Multidisciplinary Optimization*, 42(5):645–663, 2010.

Erik H Vanmarcke. Matrix formulation of reliability analysis and reliability-based design. *Computers & Structures*, 3(4):757–770, 1973.

Sergio Verdu and H Poor. On minimax robustness: A general approach and applications. *IEEE Transactions on Information Theory*, 30(2):328–340, 1984.

David C Viano, Ian V Lau, Corbin Asbury, Albert I King, and Paul Begeman. Biomechanics of the human chest, abdomen, and pelvis in lateral impact. *Accident Analysis & Prevention*, 21(6):553–574, 1989.

Geoffrey S Watson. Smooth regression analysis. *Sankhyā: The Indian Journal of Statistics, Series A*, pages 359–372, 1964.

Lauren K Wood, Carl S Miller, Nathaniel H Madura, Matthew P Reed, Lawrence W Schneider, Kathleen D Klinich, and Jonathan D Rupp. Response and tolerance of female and/or elderly pmhs to lateral impact. Technical report, SAE Technical Paper, 2014.

Jun Wu, Jingwen Hu, Matthew P Reed, Kathleen D Klinich, and Libo Cao. Development and validation of a parametric child anthropomorphic test device model representing 6–12-year-old children. *International journal of crashworthiness*, 17 (6):606–620, 2012.

Mingdi You, Eunshin Byon, Jionghua Jin, and Giwhyun Lee. When wind travels through turbines: A new statistical approach for characterizing heterogeneous wake effects in multi-turbine wind farms. *IISE Transactions*, 49(1):84–95, 2017.